Agricultural and Forest Meteorology 378 (2026) 110978

Contents lists available at ScienceDirect

Agricultural and Forest Meteorology

journal homepage: www.elsevier.com/locate/agrformet

Future viability of European vineyards using bioclimatic climate analogues

Héloïse Allaman [a,*], Stéphane Goyette [a], Pierre-Henri Dubuis [b], Jérôme Kasparian [a]

[a] Group of Applied Physics and Institute for Environmental Sciences, University of Geneva, Bd. Carl-Vogt 66, 1205 Geneva, Switzerland
[b] Agroscope Changins, Rte de Duillier 60, 1260 Nyon, Switzerland

ARTICLE INFO

Keywords:
Viticulture
Climate analogues
Climate twins
Bioclimatic indices
Climate change
Pathogens
Subgrid-scale effects

ABSTRACT

Climate change is reshaping the geography of viticulture, threatening traditional wine regions while opening opportunities for new ones. This study applies a climate analogues approach to assess how European vineyards may evolve and/or shift under future climate scenarios. We tailor the method to viticulture by integrating bioclimatic indices related to vine growth and disease risks, correcting for vineyard-scale topography, and accounting for redundancy between the indices.

Our analysis supports both adaptation, by identifying present-day locations resembling future vineyard climates, and prospective expansion, by revealing regions with emerging suitability. We find that temperature-related indices related to plant growth drive north–south and elevation shifts, while pathogen-related indices-linked to humidity and precipitation-cause notable east–west displacements. While northern Europe may become thermally suitable for vine-growing by the end of the 21th century, its projected high humidity could intensify disease pressure, potentially limiting its long-term sustainability.

1. Introduction

Climate change has already and will continue to have far-reaching impacts across various sectors, with agriculture being one of the most affected. Among the agricultural sectors, viticulture stands out due to its deep connection to regional economies and traditions, and the repercussions of climate change on this sector are a matter of increasing concern, since grape quality and yield are highly sensitive to climate (van Leeuwen and Darriet, 2016). In some regions, the temperatures are projected to grow beyond the grape productivity range. Conversely, areas that were previously unsuitable for viticulture may become more favourable as they warm, potentially altering the global distribution of wine production (Jones et al., 2012). Alongside temperature changes impacting the vine growth and grape production, the spread of pathogens such as downy mildew, powdery mildew, and flavescence dorée has become an increasing threat to vineyard crops (Francesca et al., 2006; Caffarra et al., 2012; Robert et al., 2011). As a result, the wine sector is expected to undergo significant transformations in the coming decades. It is crucial to have tools to better describe and anticipate these changes and enable to adapt effectively to the projected climate conditions (Mozell and Thach, 2014).

The climate analogues approach, also known as the climate twins approach, is an efficient way to address these needs. The methodology consists of matching projected climates at a location of interest with those of other regions in the present (Ungar et al., 2011; Rohat et al., 2017). Climate analogues have been applied in agricultural research to identify crop varieties that are better suited to projected climate conditions and to assess existing adaptation strategies (Webb et al., 2013; Ramírez Villegas et al., 2011). This method operates on the premise that the projected climate of the considered region will mirror the current climate of another, enabling farmers to adopt best practices from areas already experiencing similar conditions. It provides insights into how shifting climates may influence the suitability of current and potential vine-growing regions. Climate analogues facilitate the identification of regions within Europe that will retain their suitability for viticulture under future climatic conditions, as well as new areas with future viticultural potential. Furthermore, it offers an intuitive way to visualize potential climate change impacts, making it accessible to both the scientific community and practitioners.

Viticulture is strongly influenced by climatic conditions, with temperature playing a key role in vine growth and grape development. Vines are particularly vulnerable to frost and extreme heat, which can cause significant and sometimes irreversible damage (Poling, 2008; Venios et al., 2020). Additionally, each grape variety requires a specific amount of accumulated heat to reach optimum ripening. This heat accumulation can be quantified using the Huglin index, a widely recognized bioclimatic index in viticulture that assesses the thermal

* Corresponding author.
E-mail addresses: heloise.allaman@unige.ch (H. Allaman), stephane.goyette@unige.ch (S. Goyette), pierre-henri.dubuis@agroscope.admin.ch (P.-H. Dubuis), jerome.kasparian@unige.ch (J. Kasparian).

https://doi.org/10.1016/j.agrformet.2025.110978
Received 25 June 2025; Received in revised form 27 November 2025; Accepted 4 December 2025
Available online 13 December 2025

conditions of a region throughout the growing season (Huglin, 1986; Piña-Rey et al., 2020). In addition to climatic constraints, vineyards are highly susceptible to various pests and diseases that can significantly impact both yield and grape quality. For instance, in 2023, an unprecedented outbreak of downy mildew affected 90% of vineyards in Bordeaux, France, with damage ranging from minor losses to complete harvest loss (Dupin and Raynal, 2024). Another growing concern is powdery mildew, which has historically been confined to Mediterranean regions but has increasingly been observed in Alsace, Champagne, and Bourgogne in recent years, related to increasing precipitation at the beginning of the growing season (Zito et al., 2019). These two main threats to vines are highly sensitive to climatic variables such as temperature, rainfall frequency, and leaf wetness duration, and are expected to become more prevalent and aggressive under projected climate change scenarios (Francesca et al., 2006; Caffarra et al., 2012). In particular, warmer and wetter springs can favour earlier infection and increase the number of disease cycles per season, amplifying disease pressure and management costs. In addition to fungal diseases, European vineyards are increasingly threatened by flavescence dorée, a bacterial disease spread by the leafhopper *Scaphoideus titanus*. First detected in Europe in the 1950s, this emerging pathogen has gradually spread northward to new regions (Abouassaf, 2013). As the development of the vector insect is closely tied to temperature and can be modelled using the degree-day method (Sneiders et al., 2019), rising temperatures are expected to accelerate its life cycle, leading to more generations per season and, consequently, a higher insect population, resulting in a higher risk of infection.

Vineyard microclimate is strongly influenced by the topography, including elevation, slope, and aspect of the terrain. These factors affect the distribution of direct sunlight and winds, which impact temperature and humidity within the vineyard (De Rességuier et al., 2020). Topography also plays a crucial role in soil properties by regulating water movement and erosion patterns (Magdić et al., 2022). These variations in temperature and moisture conditions directly influence vine growth and disease incidence. As a result, topography is a key parameter in viticulture, so that vineyards are often planted in hilly regions and on south-facing slopes (in the northern hemisphere) to optimize sunlight exposure, especially in northern vineyards. The spatial scale of topography lies below 100 m, much finer than the typical 10 km grid size of the most resolved available regional climate models. However such fine scale is essential for accurately describe the climatic conditions necessary for vine growth and to ensure a reliable assessments of vineyard suitability.

Despite the valuable insights climate analogues can offer in helping wine-growers assess and adapt to climate change, their application to the study of vineyard shifts has remained relatively limited. Webb et al. (2013) conducted a study applying the climate analogue approach to viticultural regions, focusing on a limited number of global sites and using only temperature and precipitation as variables. In contrast, our study operates at both the scale of individual vineyards and the regional level, encompassing all wine-growing regions of Europe. We introduce a climate-matching approach tailored to the climatic and topographic conditions of European vineyards. By incorporating several bioclimatic indices rather than the raw physical parameter provided by climatic models, we directly account for key factors influencing both grape growth and the development of vineyard diseases. We consider sub-grid topography by calculating local temperature corrections based on slope, aspect, and elevation. We then extend our analysis beyond the matching of individual vineyards, identifying climate analogues of wine regions, revealing consistent mappings from region to region. We consider both the adaptation of existing vineyards to their projected future conditions and the potential emergence of new vine-growing regions as a result of climate change. We show that the consideration of pathogens drastically restricts the regions subject to such emergence.

2. Methods

Vineyard analogues are computed for the periods 2006–2035 and 2066–2095, referred to by their central years 2020 and 2080. Section 3.5 also includes intermediate horizons, with analogues evaluated between 2006–2035 and 2026–2055 (labelled 2020 and 2040) and between 2006–2035 and 2046–2075 (labelled 2020 and 2060).

2.1. Data sources

The locations of European vineyards are obtained from the CORINE Land Cover database (CLC), which provides comprehensive land use information across Europe (European Environment Agency, 2018; European Union's Copernicus Land Monitoring Service, 2025). The dataset, dating from 2018, has a resolution of 25 hectares (500 m × 500 m) for areal phenomena, such as vineyard plots. Vineyards are represented as polygons. We identify each closed plot as an individual vineyard, yielding a total of 21,076 vineyards. For each plot, the centroid is extracted using the *native:centroids* function from the QGIS (Quantum Geographic Information System) software (QGIS, 2024). This centroid is then used as the vineyard's representative location.

The topographic data are extracted from the European Digital Elevation Model (EU-DEM) provided by Eurostat, which has a resolution of 25 m (Copernicus Land Monitoring Service and European Commission, 2013). For each vineyard, elevation, slope, and aspect are determined based on the DEM point closest to the vineyard's centroid.

The climate data used in this study are extracted from the CORDEX (Coordinated Regional Climate Downscaling Experiment) database (Jacob et al., 2014). Six key variables are considered: near-surface air temperature (average, maximum, and minimum), precipitation, near-surface relative humidity, and surface downwelling shortwave radiation, all provided at a daily resolution. The selected domain is EUR-11, which covers the entire European continent with a spatial resolution of 12 km. For this analysis, we use climate projections from the Danish Meteorological Institute (DMI) using the HIRHAM5 (Christensen et al., 2007) regional climate model (RCM) under the RCP8.5 emissions scenario. We focused on the RCP8.5 scenario because it provides the largest climate forcing among available scenarios, thereby highlighting potential long-term impacts on European vineyards and enabling a robust analogue-based analysis. This model has proven to produce reliable climate simulation over Europe (Jacob et al., 2007). The dataset spans the period 2006 to 2095. The historical period (2006–2024) is also based on simulations from the HIRHAM5 RCM, to allow consistent matching with the future projections. The climate data are obtained at each vineyard location using a bilinear interpolation from the four nearest grid points from the RCM dataset relative to the vineyard's centroid. The elevation difference between the vineyard provided by EU-DEM and the interpolated elevation of the HIRHAM grid cell, as well as the slope and aspect of the terrain are then considered to adjust the temperature at the vineyards locations, as detailed in the next subsection.

2.2. Local temperature correction for sub-grid topography

The interpolation of average, maximum and minimum near-surface air temperatures at vineyard sites from the grid cell of the model output omits the impact of topography. A correction is therefore applied to the temperature for both elevation and slope.

The temperature variation with elevation is given by:

$$T_{\text{vine}} = T_0 + \Gamma_e(z - z_0), \tag{2.1}$$

with $\Gamma_e = -0.0065$ °C/m the environmental lapse rate, and z the elevation of the vineyard (Peixoto and Oort, 1992). T_0 and z_0 are the interpolated values extracted from the four nearest neighbours of a vineyard on the computing grid.

The slope and aspect correction accounts for enhanced solar exposure on south-facing slopes in the Northern Hemisphere, which receive more direct sunlight and thus tend to be warmer. The correction is the following (Bennie et al., 2008):

$$T_{\text{slope}} = T_{\text{flat}} + a(1-\alpha)(R_{\text{sw}}^{\text{slope}} - R_{\text{sw}}^{\text{flat}}), \tag{2.2}$$

with $a = 0.013$ a dimensionless coefficient considering a typical wind speed $u \geq 1$ m/s, $\alpha = 0.2$ the surface albedo of the vineyard (Pieri and Gaudillère, 2015), T_{flat} the temperature on a flat surface receiving a net shortwave radiation flux $R_{\text{sw}}^{\text{flat}}$, and T_{slope} the temperature on a slope at the same location receiving a radiation flux $R_{\text{sw}}^{\text{slope}}$. The net shortwave radiation flux received by a flat surface $R_{\text{sw}}^{\text{flat}}$ depends on the sun incidence, which is a function of the time and the day. We estimate it from the daily flux provided by the RCM, by assuming that the cloud cover is constant throughout the day. The radiation flux is therefore given by a fraction of the clear-sky solar radiation $R_{\text{cs}}^{\text{flat}}(t)$:

$$R_{\text{cs}}^{\text{flat}}(t) = F_s \cdot r^{*2} \cdot \psi^{\sec Z(t)} \cdot \cos Z(t), \tag{2.3}$$

$$R_{\text{sw}}^{\text{flat}}(t) = \frac{\bar{R}}{\bar{R}_{\text{cs}}} R_{\text{cs}}^{\text{flat}}(t), \tag{2.4}$$

with $F_s = 1370$ W m^{-2} the solar constant, r^* the relative deviation from the Earth–Sun distance with regard to its average value, $\psi = 0.75$ the atmosphere transmissivity at mid-latitudes, $Z(t)$ the solar zenith angle, $\bar{R}$ the daily average solar radiation obtained from the climate model given the cloud cover, and $\bar{R}_{\text{cs}}$ the clear-sky solar radiation on a flat surface averaged over 24 h. The solar radiation $R_{\text{sw}}^{\text{slope}}$ received on a slope is a function of the slope S and the aspect Ω of the surface, but also the angle of the sunbeam with regard to the terrain (Oke, 1987). Thus, it depends on the time t of the day and is estimated by:

$$R_{\text{sw}}^{\text{slope}}(t) = \frac{R_{\text{sw}}^{\text{flat}}(t)}{\cos Z(t)} \left(\cos Z(t) \cos S + \sin Z(t) \sin S \cos\left(\Omega_S(t) - \Omega\right)\right), \tag{2.5}$$

where $\Omega_S(t)$ is the solar azimuth. The solar azimuth and zenith angles can be computed using spherical geometry (Oke, 1987). They depend on the latitude, date, and time, leading to different correction magnitudes for the average, maximum and minimum near-surface air temperature, respectively. Indeed, the daily minimum temperature, which is reached at nighttime, is expected to be marginally affected by the slope, while the correction to the daily maximum temperature will be maximal, since it is reached close to zenith. In order to calculate this correction, we use the maximum solar radiation, reached at solar noon, when Z is locally the lowest. The correction of the daily mean temperature is then obtained by computing the hourly temperature correction and averaging over 24 h.

In order to pair the projected climate of vineyards to RCM grid points in the present, we also correct the temperature of the RCM grid point for the most likely location of vines. Each cell is roughly 140 km^2 and may cover a wide range of topographic conditions. As vines tends to be located on south-facing slopes, we seek for climate analogues at such location. For each grid cell, we therefore consider the location that maximizes the correction of the daily maximum temperature. Note however that this approach could also point to areas that may become too hot for successful viticulture in others, therefore preventing potential matches, especially in the southern part of the considered region.

2.3. Bioclimatic indices

In order to describe the climate suitability for vine-growing, we rely on six bioclimatic indices. Three of them consider climate conditions relevant to the growth of vine and three other to pathogens development. Optimal climatic conditions for vine growth must be maintained throughout the growing season, from bud break to harvest. Thus, we first estimate of the bud break day (BB), which depends on the quantity of heat received by the vine. It can be estimated using growing degree-days, starting from January 1st (01 Jan) (Garcia de Cortazar-Atauri et al., 2009):

$$\sum_{01\ \text{Jan.}}^{BB} \max\left(T_{\text{d}} - 5\ ^\circ\text{C},\ 0\ ^\circ\text{C}\right) \geq 275\ ^\circ\text{C}, \tag{2.6}$$

with T_{d} the daily mean temperature. Different grape varieties may have slightly different bud break thresholds, and selecting later-ripening varieties can reduce the risk of spring frost damage. For consistency, we applied a uniform definition across the domain. Furthermore, the specific varieties that will be cultivated in future vineyards can only be assumed, which prevents us to effectively take this information into account. We checked that the choice of this threshold defining the bud break does not impact the results.

Vine growth indices

Bare vine growth is characterized by the Huglin index (HI), which is widely used in viticulture to assess the thermal conditions of a region during the growing season (Piña-Rey et al., 2020). It calculates the cumulative heat during the growing season of the plant, from bud break day to harvest (end of September, 30 Sep.) (Huglin, 1986):

$$I_{\text{HI}} = \sum_{BB}^{30\ \text{Sep.}} \max\left[\left(\frac{T_{\text{d}} + T_{\text{max,d}}}{2} - 10\ ^\circ\text{C}\right), 0\right] \cdot K_{\text{lat}}, \tag{2.7}$$

where $T_{\text{max,d}}$ is the maximum daily temperature, and the mean between T_{d} and $T_{\text{max,d}}$ is a proxy of the daytime mean temperature. K_{lat} is a coefficient accounting for the day duration at a given latitude, given by:

$$K_{\text{lat}} = 2.55 \cdot 10^{-4} \cdot L_s + 0.278, \tag{2.8}$$

with L_s the total season day-length, i.e. the sum of daily daylight hours from bud break day to the end of September. The coefficients have been derived by Hall and Jones (2010), and fitted to match our definition of the growing season. Suitable values of HI range from 1500 to 2500 degree-days depending on the grape variety. For example, a minimum HI of 2200 is required for the Carignan variety, 1900 for the Merlot variety and 1500 for the Müller-Thurgau variety (Huglin, 1986).

The two other indices related to the impact of air temperature on vine growth are the number of frost and of extreme heat days respectively. Spring frost events are particularly damaging because they occur after the onset of bud burst, a phenological stage during which grapevine tissues are highly sensitive to freezing. Starting from bud break, low temperatures can freeze the water inside the tender tissues of the young buds, shoots, and leaves, causing cell rupture and irreparable damage. Depending on the timing and severity of the frost, damage can lead to partial or complete destruction of the primary shoots, which bear the majority of the fruiting potential. In such cases, the vine may activate secondary buds, which typically have lower fertility, resulting in reduced yield and uneven grape ripening (Fennell, 2004). In extreme cases, frost damage can lead to total crop loss and long-term structural weakening of the plant.

Injury is likely to occur when the daily minimum temperature $T_{\text{min,d}}$ ranges from −2 to −4 °C, depending on the grape variety and the duration of the frost episode (Poling, 2008; Fennell, 2004). In this work, a day is considered as a frost day if $T_{\text{min,d}} \leq -2$ °C. The risk is evaluated until the end of May, where frost is no longer expected:

$$I_{\text{frost}} = \sum_{BB}^{31\ \text{May}} \chi(T_{\text{min,d}} < -2\ ^\circ\text{C}), \tag{2.9}$$

with χ the indicator function, being 1 the condition in parenthesis is fulfilled and 0 otherwise. We checked that this definition of the frost index is strongly correlated with the probability of experiencing at least one frost event per year, i.e. the proportion of years with at least one frost event ($R^2 = 0.76$), with an average of four frost days per frost year on average. It is also strongly correlated with frost indices computed using alternative thresholds of 0 °C ($R^2 = 0.79$) and −4 °C ($R^2 = 0.85$).

Finally, while local microclimatic effects such as cold air pooling or variety-specific phenology are not explicitly resolved in this large-scale analysis, relative comparisons across decades are robust to the precise threshold chosen, and using alternative definitions would not change the overall results.

Extreme heat also poses significant risks to vineyards. When temperatures rise above optimal levels, vines experience heat stress, which can disrupt photosynthesis, slow down sugar accumulation, and impair the development of flavours and aromas in the grapes. Excessive heat can also cause dehydration and sunburn on grape skins, leading to poor fruit quality and reduced yields. The optimal daytime temperature is below 30 °C (Keller, 2020). The plant activates its heat acclimatation mechanisms at 35 °C, with already detrimental effects on yields (Venios et al., 2020). We therefore consider this threshold in the present work, and use the number of days where 35 °C is reached as the heat index:

$$I_{\text{heat}} = \sum_{BB}^{30\ \text{Sep.}} \chi(T_{\text{max,d}} > 35\ ^\circ\text{C}). \tag{2.10}$$

Pathogens indices

The three diseases and pathogens taken into account are the flavescence dorée, the downy mildew and the powdery mildew. Flavescence dorée is a grapevine disease caused by *Candidatus Phytoplasma vitis* and transmitted by the *Scaphoideus titanus* vector (Rigamonti et al., 2011). Recent studies have shown that rising temperatures associated with climate change are facilitating the northward expansion of its range, increasing the risk of flavescence dorée outbreaks in previously unaffected wine-growing areas (Stillson et al., 2020). This leafhopper develops when temperatures exceed 8.7 °C. To monitor the associated risk of flavescence dorée, the degree-days above this temperature threshold is computed. The index tracks the accumulation of heat units over time and helps to determine the number of insect generations over the season, providing insight into the timing and severity of the disease risk in vineyards. The index is given by (Sneiders et al., 2019):

$$I_{\text{FD}} = \sum_{year} \max\left[\left(\frac{T_{\text{d}} + T_{\text{max,d}}}{2} - 8.7\ ^\circ\text{C}\right), 0\right]. \tag{2.11}$$

Downy mildew is a fungal disease that affects grapevines, caused by the pathogen *Plasmopara viticola*. The disease primarily targets the leaves, stems, and grape clusters, causing typical lesions on leaves, inflorescence and bunches, and reduced fruit yield and quality. Downy mildew is most active during warm periods with high humidity as the spores require free water to infect the vine. Thus, an infection can occur if the leaves or clusters are wet, i.e. if the precipitations are sufficient, or in presence of strong dew. This last condition is not directly provided as a climate model output. We therefore estimate it by reconstructing the hourly temperature $T(h)$ from the daily minimum and maximum temperature (Wann et al., 1985). This allows to compute the time-dependent dew-point $T_{\text{dew}}(t)$ using the Magnus formula (Zito et al., 2020). The risk of infection for each day of the growing season is then given by:

$$\text{Risk}_d = \begin{cases} 0 & T_{\text{d}} < 12\ ^\circ\text{C}, \\ 1 & T_{\text{d}} \geq 12\ ^\circ\text{C and } pr \geq 1\ \text{mm/d}, \\ \frac{1}{24}\sum_h \chi(T(h) - T_{\text{dew}}(h) \leq 5\ ^\circ\text{C}) & \text{otherwise}, \end{cases} \tag{2.12}$$

with pr the daily precipitations. The sum is performed over each hour h of the day. An hour is considered at risk if the leaves are wet, i.e. if the temperature is within 5 °C of the dew point. Finally, the downy mildew index is the number of days during the growing season that are favourable for infection. It is obtained by summing over all the days that are at risk during the growing season:

$$I_{\text{DM}} = \sum_{\text{BBCH13}}^{30\ \text{Sep.}} \text{Risk}_d. \tag{2.13}$$

The BBCH13 stage is the three leaves stage, and correspond to the start of the risk period for the powdery mildew infection. It is estimated to happen 5 days after BB (Garcia de Cortazar-Atauri et al., 2009).

Powdery mildew is another common fungal disease in vineyards, caused by *Erysiphe necator*, that affects leaves, shoots, and grape clusters. It thrives in warm and humid but non-condensing conditions. Indeed, it is inhibited by liquid water on leaf surfaces, whether from rain or dew (Olivier Viret, 2025). In these cases, the spores are washed off, limiting their spread and disrupting the disease's development. It develops best when the temperature is between 8 and 32 °C, with an optimum around 24 °C (Fessler and Kassemeyer, 1995). Furthermore, the risk of infection increases linearly with moisture, until it reaches a plateau around 85% RH (Carroll and Wilcox, 2003). The powdery mildew index can therefore be expressed as (Walter Kast, 2009):

$$I_{PM} = \sum_{\text{BBCH13}}^{30\ \text{Sep.}} (f_{\text{temp}} \cdot f_{\text{hum}} - f_{\text{wet}}) \cdot f_{\text{on}}, \tag{2.14}$$

with all functions normalized to 1. Similarly to the downy mildew index, the powdery mildew index indicates the number of days during the growing season that are conducive to a powdery mildew infection. f_{temp} and f_{hum} are functions describing the optimal temperature and humidity conditions required for the disease to develop, as discussed above (Carroll and Wilcox, 2003; Walter Kast, 2009):

$$f_{\text{temp}} = 1.63 \cdot (0.11\ T_{\text{d}} - 0.0025\ T_{\text{d}}^2 - 0.6), \tag{2.15}$$

$$f_{\text{hum}} = \min\left(\frac{\text{RH}_{\text{d}}}{85}, 1\right), \tag{2.16}$$

with RH_{d} the daily mean relative humidity. f_{on} describes the ontogenetic resistance of grapes, which is high around blossom period and decreases afterwards. It is given by (Walter Kast, 2009):

$$f_{\text{on}} = \min\left(\frac{1}{100}\left(0.0002D^3 + 176.6\sqrt{D} - 114.9\ln D - 14D - 66\right), 0.2\right), \tag{2.17}$$

where D represents the number of days since BBCH13. The function f_{wet} describes leaves wetness, and is subtracted since it reduces the risk of infection. It is a composite function depending on precipitation, as well as dew, $f_{\text{wet}} = f_{\text{pr}} \cdot f_{\text{dew}}$ (Walter Kast, 2009), with:

$$f_{\text{pr}} = \frac{3}{1 + \exp(-0.5(\text{pr} - 6.25))}, \tag{2.18}$$

$$f_{\text{dew}} = \frac{1}{24}\sum_h \chi(T(h) - T_{\text{dew}}(h) \leq 5\ ^\circ\text{C}). \tag{2.19}$$

The six bioclimatic indices are computed for the whole period from 2006 to 2095. They are then averaged over each 30-year period of interest. Each 30-year period is labelled by its central year; for instance, 2040 corresponds to the period 2026–2055.

2.4. Indices aggregation

In order to define the similarity between the climate at two locations and/or times, we use the standardized Euclidean distance (SED), a common method used in the filed of climate analogues (Rohat et al., 2017; Bulut et al., 2025). The SED between a vineyard j in the future and a grid point i in the present is computed as:

$$SED_{ij}^2 = \sum_{k=1}^{N} \frac{(p_{ik} - f_{jk})^2}{s_j^2}, \tag{2.20}$$

where p_{ik} is the value of index k at the grid point i in the current climate, f_{jk} is the value of index k at the vineyard location in the future climate, and s_j is the spatial standard deviation of the index among the vineyards. The sum is performed over all N indices considered.

To address the partial redundancy between our indices, which all depend on daily mean, maximum and minimum temperature, relative

humidity and precipitations, we apply a Principal Component Analysis (PCA) (Vidal et al., 2012). It transforms the original indices into a new set of uncorrelated variables called principal components, providing an efficient representation of the dominant modes. After transforming the data into this new coordinate system, we recalculate the Euclidean distance between points, applying weights corresponding to the fraction of the variance explained by each principal component. The principal components derived from the six indices are presented in Table A.1.

Before interpreting the location of the analogues, it is essential to ensure that each analogue truly shares similar climatic conditions with the vineyard of interest. While the method identifies the best match within the study domain for each vineyard, this does not necessarily guarantee a high-quality match. We define a similarity index:

$$SI = \frac{1}{1 + d^2} \tag{2.21}$$

where d represents the PCA-adjusted SED between a vineyard and its analogue. This index ranges from 0 to 1, with 1 indicating a perfect match between climates. The decay of similarity index with the analogue rank is very progressive and SI values remain acceptably high for several analogues, with no obvious cut-off ($SI \geq 0.9$ for 92% of the 20 best analogues of all the European vineyards). Since the closest analogues of a vineyard may be widely dispersed, selecting only the single best analogue would limit the robustness of our analysis. Considering instead the 5 or 20 best analogues yields similar region-level matches. As the cut-off is not critical, we adopt five analogues per vineyard as a trade-off between robustness and clarity.

2.5. Region matching

We have grouped European vineyards into 57 regions defined by rectangles in the latitude–longitude plane, based on climate homogeneity, analogue behaviour homogeneity (i.e. most vineyards from one region having their analogues in a single or very limited number of regions) as well as geographical indications (Fig. 1). The coordinates of the regions are found in Table B.1.

Now we want to find a systematic way of defining analogues at the regional scale. This mapping should be consistent with the analogue at the vineyard scale, i.e. a region B containing most analogues of region A should be considered the analogue of region A.

For each future region A of interest, each present region B is assigned a similarity score $S_{A,B}$ given by:

$$S_{A,B} = \frac{n_{A,B}}{\sqrt{\mathcal{A}_B}}, \tag{2.22}$$

where $n_{A,B}$ is the number of analogues of the future region A present in the analogue region B and $\mathcal{A}_B$ its area. Regions with the highest scores are then considered the best matches for the region A of interest.

3. Results

3.1. Bioclimatic indices

The six bioclimatic indices considered in this work have been computed for each European vineyard for the whole period between 2006 and 2095. This section aims to analyse the values of these indices, as well as their evolution over time. Fig. 2 shows the values of the indices of European vineyards in 2020, as well as their evolution between 2020 and 2080.

Figs. 2a and 2b shows the Huglin index of European vineyards. In 2020, values range from 400 to 3500, but the plot has been caped to [1000, 2600], which accounts 95% of vineyards. About 7% of vineyards have a Huglin index below 1500 degree-days, and 4% exceed 2400, placing them outside the typical range for vine viability. This discrepancy may stem from our definition of the Huglin index (Eq. (2.7)), which is calculated from bud break, whereas it is conventionally computed from a fixed date in the literature (Huglin, 1986; Piña-Rey et al., 2020). It may also result from local temperature corrections, which – despite being included – might be insufficient in some cases, or from the interpolation of temperature from the four nearest grid points of the RCM, which can be inaccurate in areas with complex topography.

The values of the Huglin index are greater for the future period in the entire domain, with an increase over the century ranging from approximately 400 in the northernmost vineyards, up to 800 in the Iberian Peninsula. As the optimal Huglin index for vine growth lies between 1500 and 2400 degree-days depending on the grape variety (Huglin, 1986), several regions, particularly Spain, Italy and Turkey, may be unable to sustain viticulture by the end of the century.

The flavescence dorée index and its evolution are displayed in Figs. 2c and 2d. The present values (panel (c)) range between 500 and 4500, with 98% of vineyards lying between 1400 and 4000. The *Scaphoideus titanus* requires about 1035 degree-days to grow from the egg to the first egg-laying, meaning a new generation emerges every 1035 degree-days (Rigamonti et al., 2011). Hence, a secondary colorbar displays the number of generations expected per year. This index follows the same trend as the Huglin index, both in 2020 and for the evolution between 2020 and 2080. Indeed, as both indices are calculated using a degree-day method, they are strongly correlated ($R^2 = 0.87$), differing only in the base temperature and the period of the year considered. The results indicate an increase in the risk of flavescence dorée for all European vineyards in the future. The index increases by more than 520 degree-days (half a generation) for over 99% of vineyards and by more than 1035 degree-days (one full generation) for 12% of vineyards. Because the insect population increases exponentially with each new generation, the occurrence of bivoltinism could lead to a major increase in infection risk, although a direct relationship has not been proven (Chuche and Thiéry, 2014). Moreover, the distribution range of the vector cicada is shifting northwards, progressively colonizing new areas. As a result, vine-growing regions that were previously unaffected may become increasingly exposed to the risk of flavescence dorée.

Figs. 2e and 2f display the number of frost days in 2020, and the change in this number between 2020 and 2080, accounting for temperature corrections. The regions that exhibit the most risk for frost are the alpine regions, Bulgaria, and Italy. The number of frost days ranges from 0 to 5 days per year, the maximum being reached in Wallis, in Switzerland. Fig. 2f has been caped to ±2 days per year, but has values ranging from −5 to 2 days per year. In most regions, no significant change is observed as the number of frost days remains zero in both periods. However, some areas, including Wallis, central Italy and Bulgaria, show a reduction in frost risk in the future. Conversely, regions such as Bordeaux and central Turkey are projected to face an increased risk of frost. This paradoxical higher risk of frost in a warming climate is due to earlier bud break, which is projected to occur before the likelihood of frost has subsided.

The extreme heat index is shown in Figs. 2g and 2h. For the present period, values can reach up to 60 days per year, with 98% of values lower than 15 days. The regions of our study area that are affected the most by extreme heat are southern Spain and southeastern Turkey. Furthermore, the number of extreme heat days is projected to increase across the entire domain, with the most pronounced impacts in regions where the risk is already high, i.e. in the Iberian Peninsula and southern Turkey. In these regions, the number of extreme heat days could rise to as many as 80 per year, compared with around 20 per year in the current period. Italy, Greece and Bulgaria will also see a significant increase in the number of extreme heat days, with an increase of between 10 and 30 days per year.

The downy mildew index at vineyard locations is shown in Figs. 2i and 2j. The index reaches values up to 160 risk days per year, corresponding to conditions favourable to the pathogen over almost the full growing season. The regions most affected by this pathogen are mainly coastal areas, where humidity is higher, as well as northern regions. In contrast, Spain and Turkey experience the lowest impact, since the

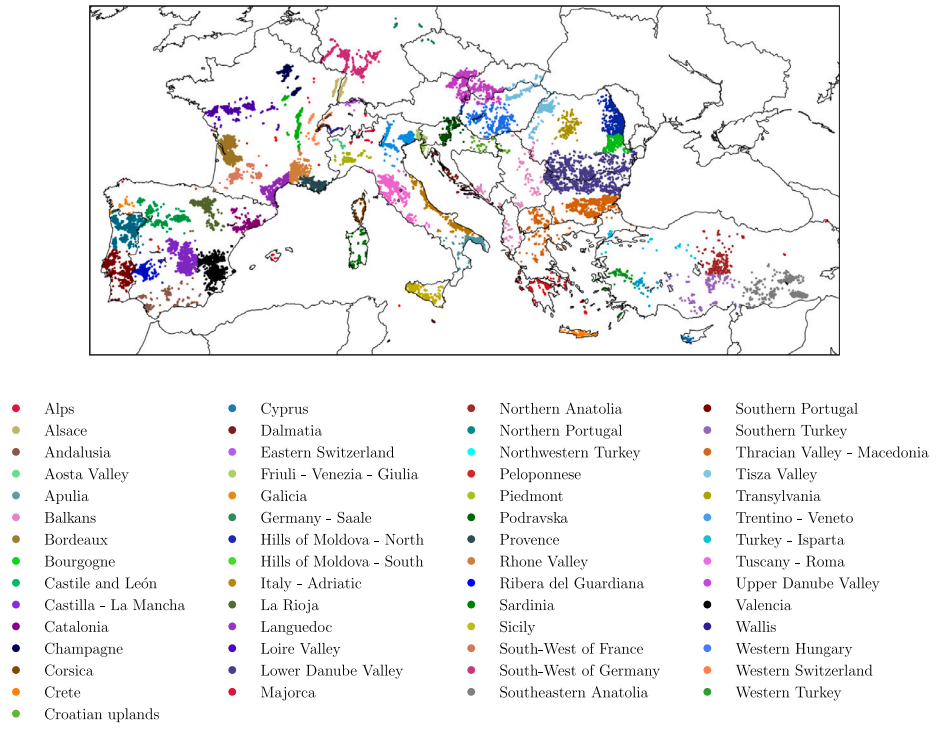

Fig. 1. Wine regions of Europe. Coloured dots correspond to individual vineyards.

climate is too dry for the pathogen to develop. Fig. 2j shows the change in downy mildew infection risk between 2020 and 2080. Values range between −50 and 40. At the end of the century, Spain, central Italy, and Eastern Europe are projected to experience a decrease in downy mildew risk due to a drier climate with reduced precipitation (Jacob et al., 2014). As a result, the number of days that satisfy the condition $pr \geq 1$ mm/d from Eq. (2.12) will decline, and relative humidity will also decrease, leading to a lower downy mildew index. Conversely, Germany, central France, Switzerland, and Turkey are expected to see an increase in downy mildew risk. Rising temperatures will lead to more days with $T_d \geq 12$ °C, while humidity levels will remain sufficient for the pathogen to develop, thereby increasing the disease pressure in these regions.

The powdery mildew index in 2020 is presented in Figs. 2k and 2l. Values range from 5 to 50 risk days per year. Similar to the downy mildew index, the risk is higher for coastal regions, especially in Portugal and southern Italy. Mountainous regions such as the Alps and the plateau of Turkey are less impacted by the pathogen. In the projected climate (Fig. 2l), the risk of powdery mildew is expected to rise across most regions, except in central Spain and southern Turkey, where temperatures will become too high for the pathogen. Evolutions across the century are comprised between −2 and 15 risk days.

Regions such as Germany, Switzerland, Bourgogne, and Champagne are anticipated to experience approximately a 15% increase in the number of days favourable to both downy and powdery mildew infections. In these areas, rising temperatures will create more favourable conditions for powdery mildew, which thrives at an optimal temperature of 24 °C, as described in Eq. (2.15). Additionally, the general decrease in precipitation across most regions during the growing season (Jacob et al., 2014) will further support the spread of powdery mildew, as the pathogen is inhibited by liquid water. This contrasts with downy mildew which is favoured by wetter conditions and higher precipitation levels.

3.2. Climate analogues of European vineyards

In the present section, we are interested in the locations of the climate analogues of European vineyards. We first focus on analogues between 2020 and 2080.

95% of the five best analogues of European vineyards are reliable, with similarity index above 0.9. 4% out of the remaining 5% are in the regions of Bordeaux, South-West of France, and Northern Anatolia, in Turkey. Indeed, as seen in Fig. 2f, these regions are projected to experience an increase in the number of frost days, due to earlier bud break days. Thus, no region within the study domain simultaneously satisfies both similar increased frost risk and comparable temperature and humidity conditions.

Fig. 3 displays the locations of the five best analogues for all European vineyards, based on their projected future conditions. The majority of these analogues are found in the Mediterranean region, with particularly high densities in southern Spain, southern France, central and southern Italy, the Balkans, western Turkey, and the eastern Mediterranean. A significant number are also located in North Africa. In contrast, northern and central Europe host very few analogues.

Examples of analogues of individual vineyards are presented in Fig. 4, showcasing different patterns of analogue distribution. For some vineyards, such as Oberderdingen (Germany) and Villamanrique de la Condesa (Spain), the first five analogues are clustered within a restricted area, forming a consistent pattern. In other cases, such as Tallya (Hungary) and Alektora (Cyprus), the first five analogues are still concentrated in one or two specific regions, or there is only one outliers. Finally, some vineyards, such as Noicattaro (Italy), exhibit no clear spatial pattern, with their analogues scattered over a wide geographical area.

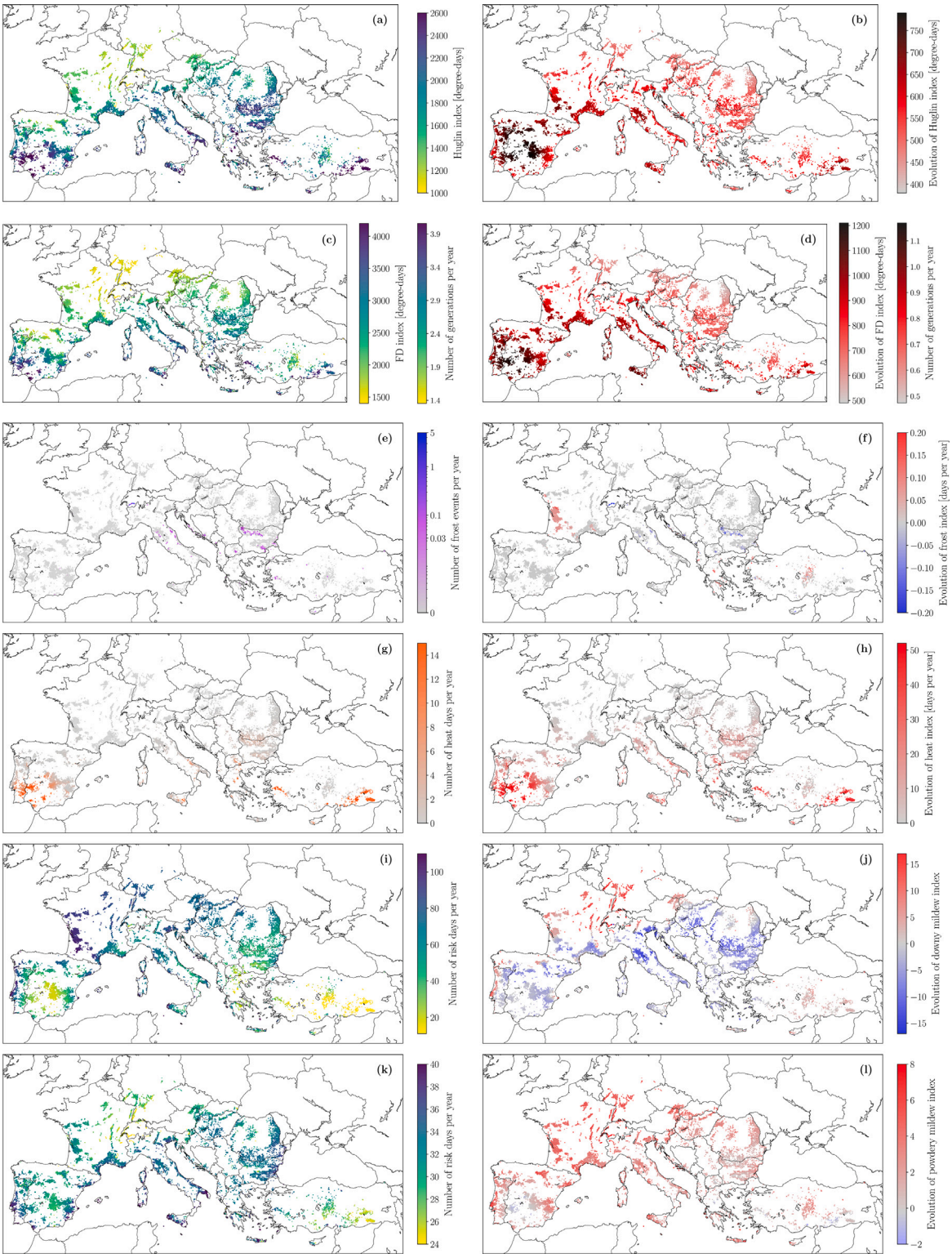

Fig. 2. Bioclimatic indices of European vineyards. Left column: values in 2020; right column: change from 2020 to 2080. **(a, b)** Huglin index; **(c, d)** Flavescence dorée (FD) index; **(e, f)** frost; **(g, h)** extreme heat; **(i, j)** downy mildew; **(k, l)** powdery mildew.

3.3. Region matching

In addition to the consistency observed between the analogues of a single vineyard, a consistent pattern emerges among multiple vineyards within the same region. This behaviour is illustrated in Fig. 5 for two regions: Champagne (France), and Ribera del Guadiana (Spain). While all analogues are displayed on the plot, only 2% of arrows have been plotted in order to maintain legibility. The similarity index lies above 0.995 for all analogues in the selected regions. Moreover, with very few outliers (less than 5% of vineyards in these two cases), most individual analogues of a given region are concentrated within two or three regions: Champagne analogues are primarily found in

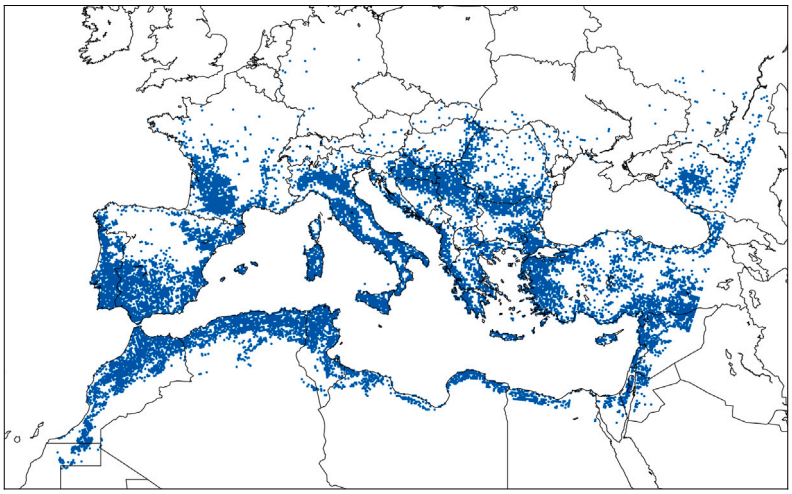

Fig. 3. Location of the five first analogues of European vineyards.

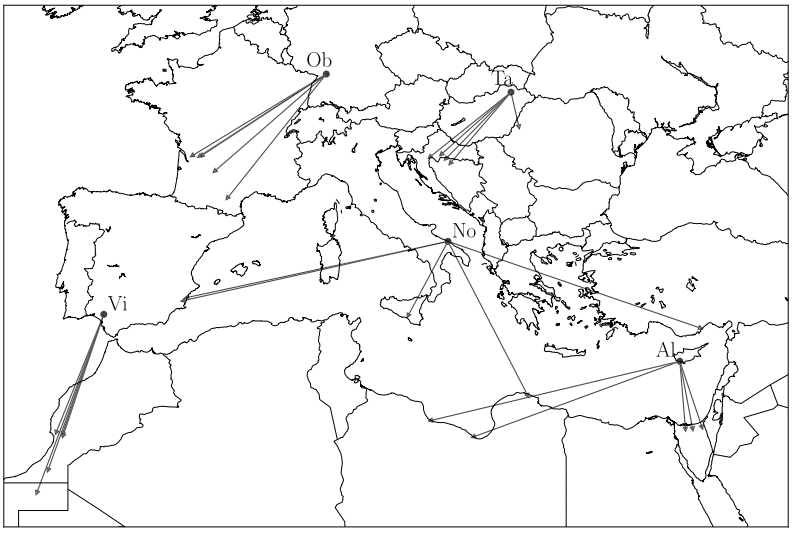

Fig. 4. Five best analogues of selected vineyards. Vi: Villamanrique de la Condesa (Spain); Ob: Oberderdingen (Germany); No: Noicattaro (Italy); Ta: Tallya (Hungary); Al: Alektora (Cyprus). The analogues are computed between 2020 and 2080.

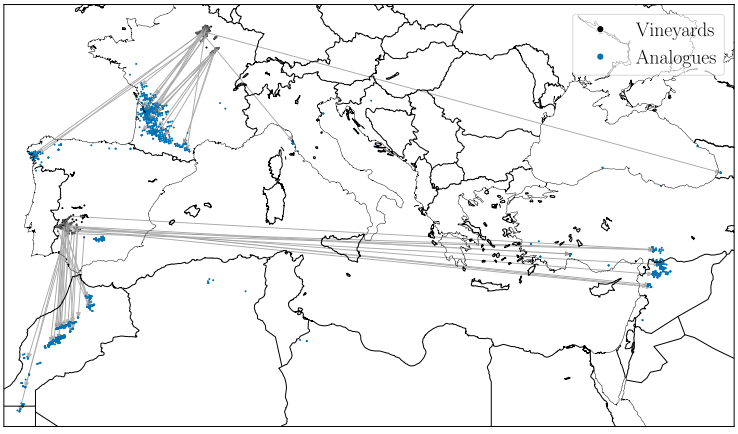

Fig. 5. The five best analogues from all vineyards in the Champagne region of France and the Ribera del Guardiana region of Spain. Analogues are computed between 2020 and 2080.

Bordeaux, South-west of France, and Galicia (Spain), while Ribera del Guadiana analogues are found in Morocco and Syria. This homogeneity is also observed in the other regions, confirming the relevance of our definition of the regions (Fig. 1), as they ensure homogeneity in analogue behaviour.

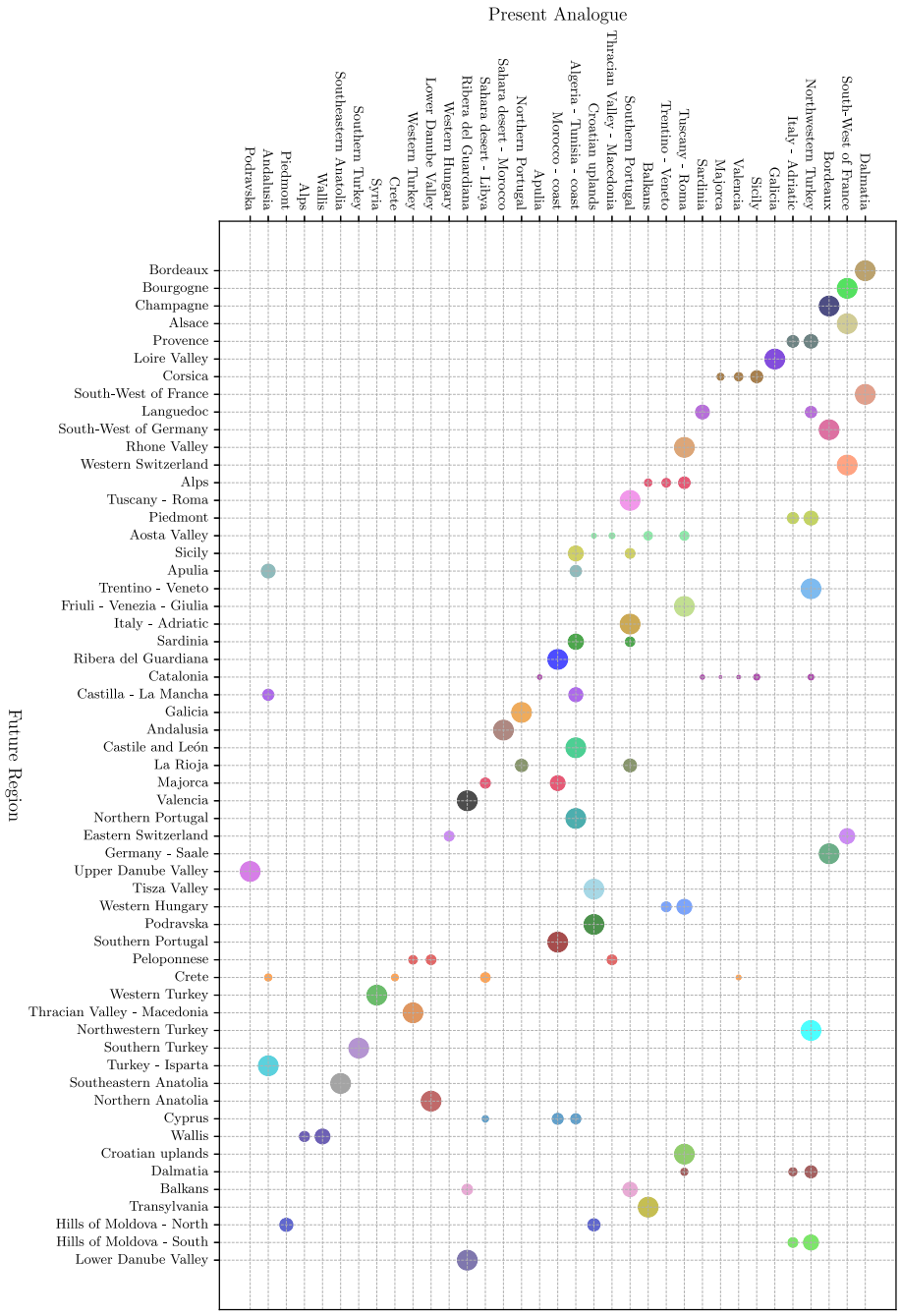

Fig. 6. Regions matches between the projected climate of vine-growing regions (left) and their analogue regions in the present (top) considering the five best analogues for each vineyard. The area of the dot is proportional to the score of the analogue region.

Fig. 6 shows the match between the projected climate of each region (left) and their analogue region in the present (top). The area of each dot is proportional to the similarity score of each region, as defined in Eq. (2.22). Matches were determined by applying Eq. (2.20) to the five best analogues for each vineyard, and an analogue region is included in the figure if its similarity score is at least 50% of the similarity score of the best matching region. Out of the 57 regions, only 30 are represented in the analogue regions. Additionally, six non-European regions are found among the analogue regions, all located in Northern Africa and the Middle East.

The maps of Fig. 7 display the best matches for each region. For each region, only the best match is shown, except for regions where the next match reaches at least 80% of the score of the first analogue region. Out of the 57 European wine-growing regions, 31 have their best analogue region located to their east, while 22 have their analogue to their west. Notably, four regions – Wallis, and three regions in Turkey – serve as their own analogue. These are mountainous areas, characterized by a high degree of topographical variability. In these cases, moving to higher elevation decreases the temperature, while maintaining a climate as similar as possible to the original one. Furthermore, 55 out of the 57 regions have their analogue located to their south, corresponding to warmer climates; the two exceptions are Northern Anatolia and the Peloponnese, where the vineyards are situated in mountainous terrain. In this case, a northern analogue does not necessarily indicate a cooler climate for these regions, but rather to a simultaneous decrease in elevation.

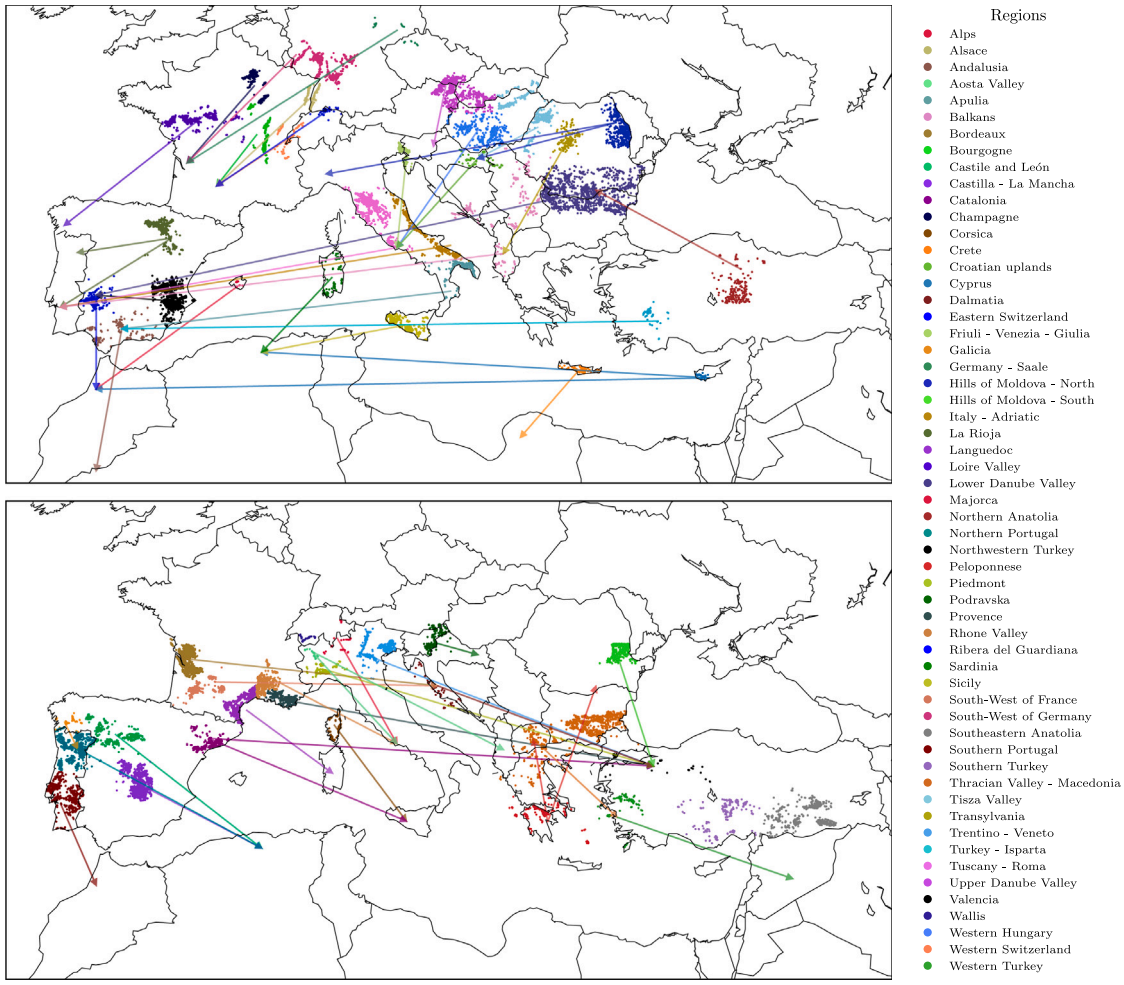

Fig. 7. Maps showing the best analogues for each region, between Europe in 2020 and existing vineyards in 2080. The regions have been distributed between the two panels according to the main direction of their migration flow, in order to maximize readability.

3.4. Contribution of each index to the pairing

To assess the robustness of the above results, we investigate how the selection of the analogues depend on the choice of the considered indices. For this purpose, analogues are computed while discarding certain indices, and compared to the analogues obtained using all six indices as in the previous sections. That way, we can assess the contribution of each index, i.e. in which direction and with what magnitude it is "pulling" the result. For this section, only the best analogue of each region is considered.

Table 1 summarizes the primary influence of all bioclimatic indices on the analogue selection process. The column "Induced analogue offset" reports the number of regions retaining the same analogue region, shifting to a region less than 500 km away, or being matched with a region more than 500 km away when the given index is included as compared to when it is not. Overall, the inclusion of either the Huglin index or the flavescence dorée index appears to result in a slight southward displacement of the analogues. These two indices are highly correlated ($R^2 = 0.87$), consistent with their relatively similar definition, both relying exclusively on temperature aggregated as growing degree-days.

For most regions, the frost and extreme heat indices have little impact on the selection of analogues. Indeed, only 15 regions have at least 10 vineyards with a frost day index greater than zero. For all other regions, the frost index has a much smaller influence on the selection of the analogue. Conversely, the regions affected by the inclusion of the frost index are those with a projected increased number of frost days in 2080, such as Bordeaux, South-West of France, and three regions in Turkey (see Fig. 2f). Indeed, while the number of frost days in 2020 is zero for those regions, it is projected to increase up to 0.2 days per year in 2080. While this value may seem small, it still represents a typical recurrence time of 5 years, assuming frost days are independent. It can therefore have a strong impact on the annual harvest. The frost index therefore plays an important role in determining the analogues of these specific regions. The regions that have a different analogue

Table 1
Contribution of bioclimatic indices to the choice of analogues: direction and distance of the analogue shift induced by considering each index, or combination of indices.

Index	Contribution	Induced analogue offset		
	to analogues	None	≤ 500 km	> 500 km
Huglin index	Southward	44	5	8
Flavescence dorée	Southward	36	5	16
Frost days	Marginal	50	0	7
Extreme heat days	Marginal	44	3	10
Downy mildew	Westward	22	5	30
Powdery mildew	Westward	31	9	17
Huglin index and Flavescence dorée	Southward	34	4	19
Downy mildew and powdery mildew	Westward	10	6	41

when including the extreme heat index are regions already impacted by heat episodes, having typically between 5 and up to 50 extreme heat days per year. They are all located in southern Europe, including four in Spain, as well as Provence, Apulia, Corsica, and Dalmatia. Given that these regions are more prone to extreme heat than those further north, the heat index has a more pronounced influence on analogue determination in southern Europe.

When downy mildew index is included, 22 regions have their best analogue located further west than the analogue obtained without it. Two third of these are regions located in the northern part of Europe, i.e. regions that are projected to experience a higher risk of downy mildew in the future, as seen in Fig. 2j. One third of the regions have analogues pulled westward by the downy mildew index despite a decrease in downy mildew risk in the future. This occurs when the analogue obtained without the downy mildew index is located in mountainous areas in the easternmost part of the domain—namely Turkey, Bulgaria, and Romania.

When the powdery mildew index is included, 11 regions find their analogue shifted westward compared to the analogue computed without it, although the effect is less pronounced than that of the downy mildew index. When both the downy and powdery mildew indices are considered, only 10 regions out of 57 retain the same analogue as without these two indices, highlighting their important role in determining the best analogue region. In addition to the increased risk of downy mildew in the northern part of Europe, most vineyards are projected to experience a higher powdery mildew pressure in the future, as depicted in Fig. 2l. For these regions, these two indices, influenced by precipitation and humidity, tend to pull analogues closer to the coast, where humidity and precipitation are generally higher and more evenly distributed in time, leading to greater pathogen pressure. Specifically, these indices play a key role in shaping the east–west displacement of analogues. However, omitting them means relying only on temperature, which reduces the constraints on analogue identification. This leads to greater dispersion of analogues among vineyards within the same region, making it harder to delineate a clear and consistent analogue region.

Hence, all indices influence the selection of analogues in different ways, making it essential to consider all of them. Focusing solely on temperature-based indices such as the Huglin index can obscure important east–west shifts driven by pathogen-related risks. Moreover, elevation plays a key role in the identification of climate analogues: while a shift in latitude may achieve the necessary temperature conditions, a shift in elevation can help to also meet specific humidity and precipitation requirements.

3.5. Intermediate time steps

The century-scale perspective exceeds the typical lifespan of a grapevine. As such, we now consider intermediate stages that align with the actionable lifespan of a vineyard, typically a few decades. This corresponds to the scale at which decisions regarding the relocation of vineyards or the replacement of grape varieties can realistically be implemented. We therefore look at the evolution of the analogues of every region over three time periods: 2020–2040, 2020–2060, and 2020–2080.

Fig. 8 illustrates examples of the typical temporal evolution of analogues for several European vine-growing regions. These regions displayed on the map were selected to represent the variety of typical trajectory patterns while excluding those that are their own analogue in at least two of the three time periods considered. The regions have been distributed between the two panels to avoid crossing arrows, and thus to improve readability. The dotted lines represent the shift in analogues between 2020 and 2040, the dashed lines between 2040 and 2060, and the solid lines between 2060 and 2080. The absence of a specific time step indicates that the analogue remains unchanged from the previous period.

37 out of the 57 regions exhibit no shift in the first period, and 10 move to neighbouring regions. As the time period progresses, however, the analogue regions become more distant. A typical trajectory for an analogue region is to remain stationary or experience minor displacements with no clear north–south pattern in the early periods, followed by larger jumps, often with a southward trend, as the considered period extends further into the future. Among the 57 regions, 24 experience only a single shift across the three time periods considered, 12 exhibit pronounced shifts first eastward and then westward (or vice versa), and 21 follow a smoother trajectory composed of two or three gradual shifts in similar directions.

Fig. 9 shows the evolution of the mean distance between individual vineyards and their five best analogues computed between 2020 and each future period of interest, and of the percentage of regions that are their own analogues. The distance increases monotonically as the time period considered increases, while the number of regions mapped to themselves decreases. More specifically, in 2040, 70% of the regions are still their own analogues. However, the percentage of regions that remain their own analogue decreases over time, reaching 7% in 2080. Furthermore, the distance between vineyards and their analogues increases by approximately 700 km over 50 years, corresponding to a climate velocity of about 15 km/year. This estimate aligns with previously reported values of climate change velocities (Loarie et al., 2009; Gaponenko et al., 2022).

3.6. Prospective wine regions

We now consider the symmetric perspective as in the previous sections: we focus on vineyards' climate in the present period (2020) and identify their analogue regions in a future time period of interest (here 2080). To identify potential future wine-growing regions, we extend our analysis beyond current wine regions by defining additional regions distributed across Europe. As with existing wine regions, these are represented as rectangles in the latitude–longitude plane. The coordinates of these prospective regions are provided in Appendix B. This approach provides insights into regions that may become suitable for viticulture in the future, and how these potential new vine-growing regions would look in relation to currently known regions and associated vine varieties and techniques.

Fig. 10 provides a map of the best prospective analogue of each region. Out of the 57 regions, 43 have their best prospective analogue region located westward of the original vineyard, and 47 northward. Five regions have an analogue at a comparable latitude, and five others to the south. These 10 regions have an analogue region is a mountainous region, such as Turkey and the Alps, allowing the vineyards to be matched to a higher elevation. In total, 24 regions find their best analogue region in a mountainous area. Indeed, of the 57 prospective analogues, 11 are located in the Carpathians, 11 in different regions of Turkey with distinctive topography and two in Alpine regions. This suggests that optimal vineyard locations are not only moving northwards, but also to higher elevations.

This trend is symmetric to the behaviour observed in Section 3.3, where two future regions had their present analogues located northward, while four mountainous regions remained their own analogues. However, the average elevation difference between current vineyards projected in the future and their present analogues was $(+58 \pm 327)$ m, i.e. no strong trend in elevation shift overall, compared to $(+642 \pm 475)$ m for prospective analogues of current wine regions. Hence, the shift in elevation is more pronounced in the case of prospective analogues, as it affects a higher number of regions with greater elevation difference. As a result, the mean distance between prospective analogues and current vineyards is smaller than the distance from current analogues to prospective climate of current vineyards, but the elevation difference is greater. Indeed, the average difference in latitude between prospective analogues and current vineyard is $+2.1° \pm 3.0°$, while the average difference in longitude is $+5.2° \pm 11.8°$. This corresponds to an overall

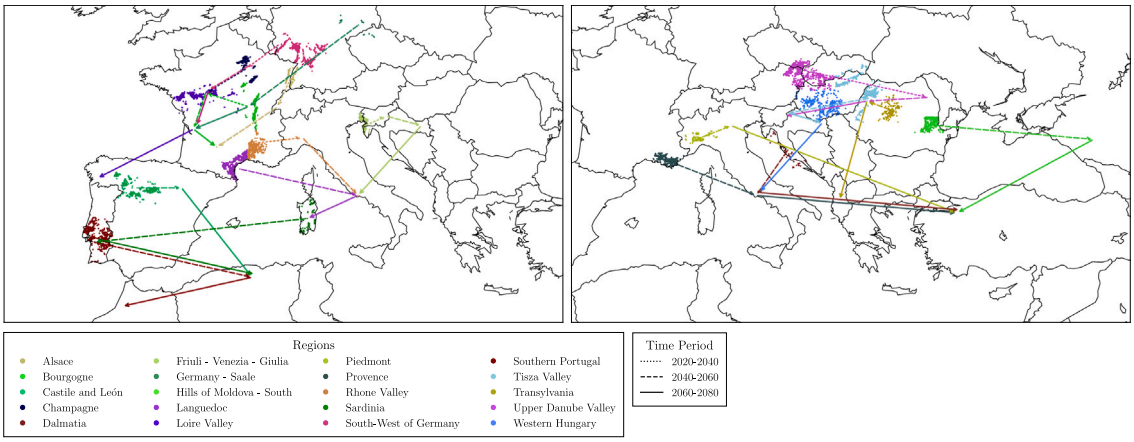

Fig. 8. Typical shift of selected vine-growing regions between 2020 and 2040, 2060, and 2080, respectively.

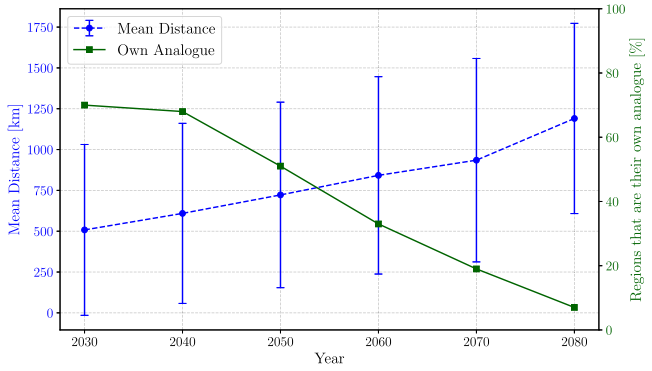

Fig. 9. Temporal evolution of the mean distance between vineyards and their five best analogues computed between 2020 and each future period of interest, and of the percentage of regions that are their own analogue.

shift of about 500 ± 800 km, about half of the distance obtained in Section 3.5 for the same time period (Fig. 9).

The tendency of prospective analogues to shift towards higher elevations rather than northwards is mainly driven by the humidity and precipitation-related indices: downy and powdery mildew. Without these indices, the mean altitude difference between current vineyards and their projected analogues reduces to (+242 ± 607) m. Fig. 11 displays the locations of the five best prospective analogues of individual European vineyards, both with and without considering the downy and powdery mildew indices. When only the four temperature-related indices are used, analogues are found across 17,179 distinct grid points, broadly distributed throughout northern Europe. In contrast, when all indices are considered, the number of distinct analogue locations drops to 11,064, with a concentration in mountainous areas such as Turkey, the Carpathians, and the Alps, as well as some locations in Eastern Europe. Furthermore, 27% of analogues are located above latitude 50 ° when considering only temperature-based indices, while this fraction reduces to 14% with all indices. The best prospective matching regions when downy and powdery mildew are omitted in comparison with the case considering all indices are found in Fig. C.1. In this case, 56 out of the 57 regions have a prospective analogue located to the north and 26 to the east of the original wine region. Thus, while temperature-related indices drive the analogues northwards, moisture-related indices mitigates this tendency, thus forcing them to migrate upwards in elevation.

The absence of European vineyard analogues in northern Europe when downy and powdery mildew indices are considered is due to the high values of the projected pathogen indices in these regions in 2080, as shown in Fig. 12. The downy mildew index has typical values between 100 and 120 risk days in regions such as England, northern France, and northern Germany, with extreme locations reaching up to 160 risk days. In 2020, it typically ranged from 10 to 100 days, with some extremes reaching 110 days along the Atlantic coast (Fig. 2i). This suggests that prospective vineyards planted in northern Europe would face an extremely high downy mildew risk in the future, at the level of the most exposed regions to date (eg. Bordeaux and South-West of France). In contrast, mountainous regions are less prone to high downy mildew risks. Similarly, the powdery mildew index is highly sensitive to topography, with significantly lower values in mountainous areas than in regions of lower elevation. For European vineyards in 2020, the downy mildew index generally ranges from 10 to 35 risk days, with occasional extremes reaching up to 40. However, projected northern Europe has powdery mildew index values between 30 and 40 risk days, with extreme values reaching 60 risk days, placing it at the upper end of today's pressure spectrum. Consequently, these two indices strongly constrain the selection of vineyard analogues, favouring locations in mountainous regions.

The restrictive effect of considering the downy and powdery mildew on the expected vine range is also illustrated in Fig. 13. It presents the current vineyards that are projected to become unsuitable for vine-growing in the future (in red) and the regions that could become climatically suitable (in green) for the periods 2040, 2060, and 2080. Fig. 13a is based solely on the Huglin index, considering a region suitable for wine-growing if its Huglin index falls within the 5th to 95th percentile range of vineyards in 2020, i.e., between 1280 and 2540 degree-days. Thus, a location is considered to become unsuitable in the future if it currently contains a vineyard but is projected to have a Huglin index above 2540 degree-days in the considered future period. Conversely, a location is classified as a potential new vineyard location if its Huglin index was below 1280 in 2020 and exceeds this threshold in the future. Fig. 13b includes our six bioclimatic indices, applying upper thresholds that correspond to the current climatic limits of most European vineyards: 0.1 frost day and 10 extreme heat days i.e. the values of the 95th percentile of the current vineyards, and 3000 degree-days for the flavescence dorée index, 85 days at risk for the downy mildew index, and 35 days for the powdery mildew index, which corresponds to the 85th percentile of the current vineyards.

For the reasons discussed above, the area projected to become suitable for vine-growth is reduced a lot when the all six indices are considered as compared to the Huglin index alone. The downy mildew condition is the strongest constraint, eliminating 25% of potential vineyard locations in 2040, 48% in 2060, and reaching 71% by 2080. This constraint alone explains the difference between Figs. 13a and 13b. For the powdery mildew, the impact is smaller but still significant, eliminating 1% of locations in 2040, 2% in 2060, and 5% in 2080.

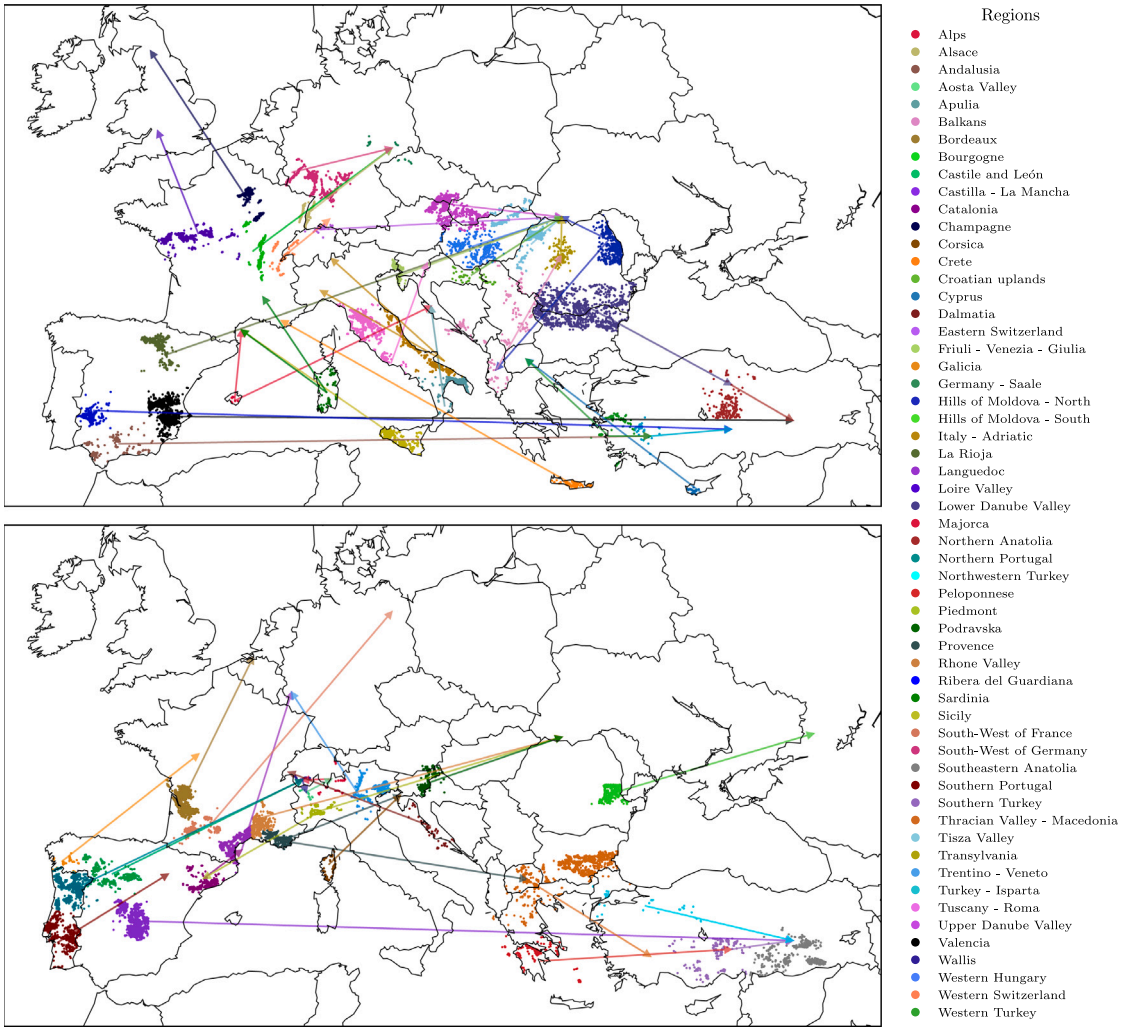

Fig. 10. Maps showing the best prospective analogues for each region, between existing vineyards in 2020 and Europe in 2080. The split of the regions between the two panels has been chosen to maximize readability.

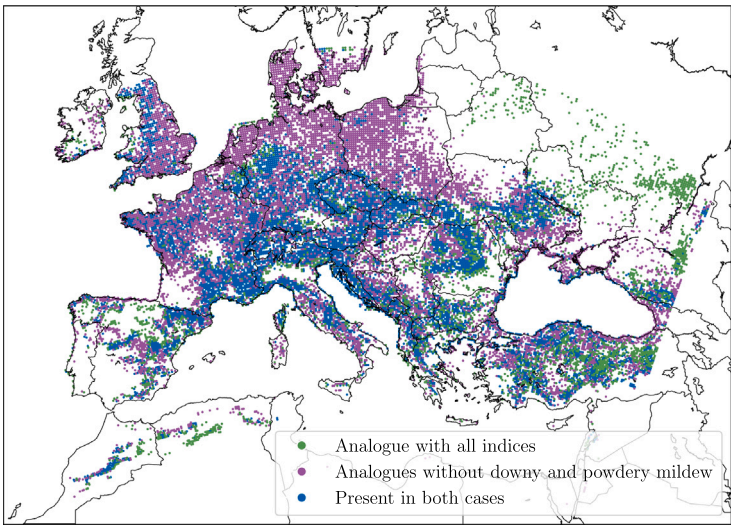

Fig. 11. Location of the first five prospective analogues of European vineyards in the present for the periods 2020 and 2080 with and without considering the downy and powdery mildew indices.

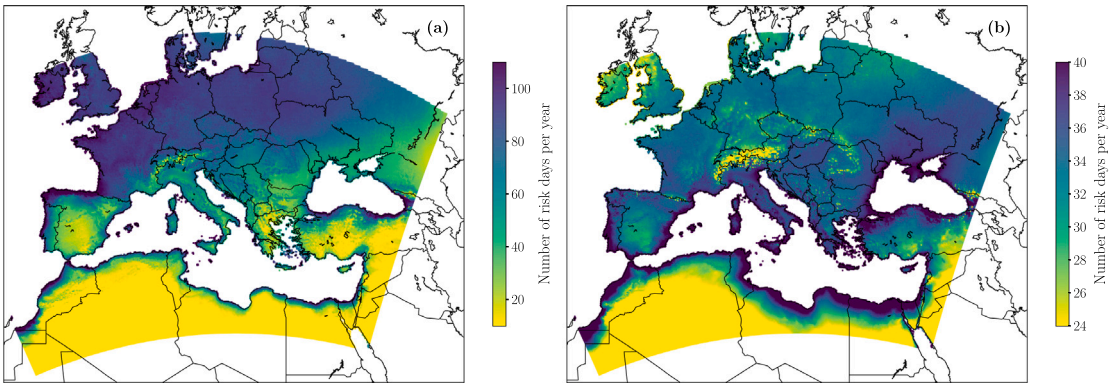

Fig. 12. **(a)** Downy mildew and **(b)** powdery mildew indices in Europe in the period 2080.

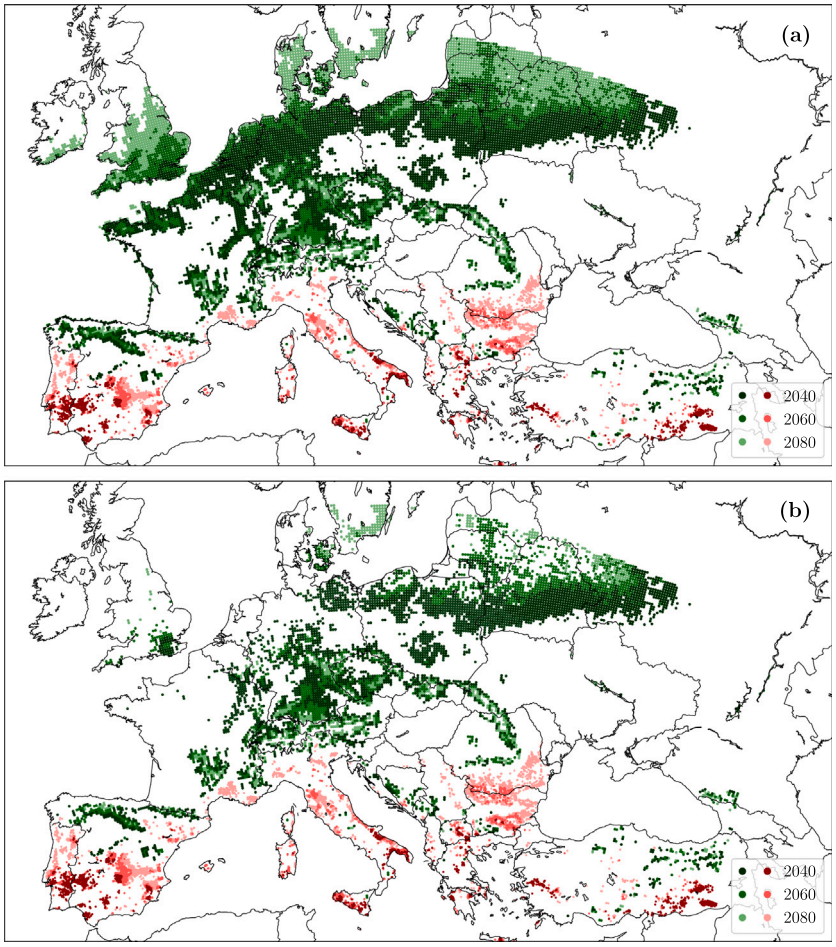

Fig. 13. Map of current vineyards projected to become unsuitable for vine-growing in the future (red), and new regions that could become suitable (green) in the periods 2040, 2060, and 2080. (a) Based on the Huglin index only. (b) Based on all bioclimatic indices.

The frost, extreme heat and flavescence dorée indices have little to no influence on the results.

The regions projected to become unsuitable for vine-growing are primarily located in southern Europe. The impacts begin as early as the 2040 period in southern Spain, Portugal, Italy, Greece, and Turkey. By 2080, central Spain and Italy, northern Portugal, Bulgaria, and southern Romania could also face conditions that make viticulture unviable. This risk impacts 46% of vineyards located below latitude 46 ° and 74% of those below latitude 40 °. These projections are only governed by temperature-related indices as precipitation and relative humidity, hence downy and powdery mildew are very low in these regions.

These results challenge optimistic projections about the establishment of vineyards in northern Europe (Malheiro et al., 2010; Nesbitt et al., 2018). While temperatures by the end of the century may become suitable for viticulture over a wide area, the increased risk of downy and powdery mildew infections raises concerns about the feasibility of growing vines on the long term in all these areas. Future vineyards in these areas will need to contend with a high pathogen threat, which could necessitate intensive disease treatments, with associated cost and environmental impact. Furthermore, while higher elevations can offer more optimal temperature and humidity conditions for vineyards, they also raise concerns regarding the availability of suitable

soil and sufficient area, as well as the accessibility and practicality of cultivating vineyards in such areas. Mountain viticulture, often on steep slopes, severely limits mechanization and leads to significantly higher production costs. In a context of overproduction and strong competition, these mountain regions are likely to face difficulties in developing profitable viticulture, as structural disadvantages such as limited mechanization, fragmented plots, and higher production costs reduce their competitiveness (Strub and Loose, 2021).

4. Conclusion

This study investigates the impact of climate change on vine growing in Europe using the climate analogues framework. Our approach is tailored to the specific requirements of vine growing by incorporating a set of bioclimatic indices, applying sub-grid climate corrections at the vineyard scale, and mitigating redundancies between indices. The bioclimatic indices cover both vine growth and pathogen development, and capture the complex climatic requirements of viticulture. Temperature-driven indices primarily cause north–south and elevation shifts in climate analogues, while pathogen-related indices incorporating moisture and precipitation, such as those for downy and powdery mildew, drive significant east–west movements. These contrasting influences emphasize the necessity of integrating all relevant indices, as each one guides the selection of climate analogues in different directions. The analysis was conducted from an adaptation perspective, finding present-day analogues for projected future climates, and from the prospective expansion point of view, identifying potential new vine-growing regions by assessing the projected climate analogues of current vineyards.

As the climate continues to warm, several regions in southern Europe may face conditions that render viticulture unviable, while northern regions will likely need to adapt their practices and grape varieties to maintain suitable conditions for wine production. Regarding prospective wine regions, while northern Europe may become thermally suitable for viticulture, our results highlight that strong disease pressure due to high projected humidity and precipitation could limit the long-term viability of vineyards in these regions. Climate change will affect more or less all current and future wine-growing regions, requiring adjustments to wine-growing areas, grape varieties and practices. While some regions may initially experience an improvement in wine quality, adjustments will be inevitable in the longer term. Adaptation will likely require trade-offs between resilience, quality, and sustainability.

CRediT authorship contribution statement

Héloïse Allaman: Writing – review & editing, Writing – original draft, Visualization, Validation, Software, Methodology, Formal analysis. **Stéphane Goyette:** Writing – review & editing, Validation, Supervision, Conceptualization. **Pierre-Henri Dubuis:** Writing – review & editing, Validation. **Jérôme Kasparian:** Writing – review & editing, Validation, Supervision, Conceptualization.

Declaration of Generative AI and AI-assisted technologies in the writing process

During the preparation of this work the authors used ChatGPT in order to improve the readability and language of the manuscript. After using this tool, the authors reviewed and edited the content as needed and take full responsibility for the content of the published article.

Funding

This research did not receive any specific grant from funding agencies in the public, commercial, or not-for-profit sectors.

Declaration of competing interest

The authors declare that they have no known competing financial interests or personal relationships that could have appeared to influence the work reported in this paper.

Acknowledgements

We acknowledge Mariana Bouvier-Rabe for her initial feasibility insights related to this work. We also thank Ronald Krause for his contribution to the development of the downy mildew index. The computations were performed at University of Geneva using HPC service. Map lines were generated using the Basemap package in Python. They delineate study areas and do not necessarily depict accepted national boundaries.

Appendix A. Principal components analysis (PCA)

A PCA is performed to account for redundancies between variables. This analysis considers all index values at all individual vineyard locations in 2080. The principal components derived from all six indices, with temperature correction applied, as detailed in Section 2.2, are presented in Table A.1. The first principal component (PC1) is mainly influenced by temperature-related indices, including the Huglin index, the flavescence dorée index, and extreme heat days, while being negatively correlated with the downy mildew index. PC1 carries a weight of 0.53, meaning it captures more than half of the total variance. The second component (PC2), dominated by the powdery mildew index, has a weight of 0.22. The third component (PC3) mainly reflects the number of frost days, with a weight of 0.16. The fourth, fifth, and sixth components each have minimal contribution, with weights below 0.07. Thus, PCA reduces the number of effective degrees of freedom from six to three while preserving the most relevant information.

Table A.1
Principal Component Analysis (PCA) of the six bioclimatic indices with temperature corrections: Eigenvectors and Weights.

	PC1	PC2	PC3	PC4	PC5	PC6
Huglin index	0.54	0.19	0.06	0.08	0.17	−0.79
Flavescence dorée	0.49	0.40	0.11	−0.07	0.54	0.55
Downy mildew	−0.44	0.32	0.11	−0.75	0.28	−0.23
Extreme heat days	0.50	−0.14	0.17	−0.58	−0.59	0.13
Frost days	−0.15	0.05	0.96	0.22	−0.08	0.00
Powdery mildew	−0.10	0.83	−0.15	0.19	−0.50	0.03
Weight	0.53	0.22	0.16	0.07	0.01	0.00

Appendix B. Coordinates of the regions

See Table B.1.

Appendix C. Prospective region analogues using temperature-related indices only

See Fig. C.1.

Data availability

The locations of European vineyards were obtained from the CORINE Land Cover database (European Environment Agency, 2018). Topographic data were extracted from the European Digital Elevation Model provided by Eurostat (Copernicus Land Monitoring Service and European Commission, 2013). Climate datasets were obtained from the CORDEX data base (Jacob et al., 2014). The Python code used to process the data is available in the Yareta repository of the University of Geneva (Allaman et al., 2025).

Table B.1
List of regions and their geographic boundaries. Regions containing several sets of coordinates are defined as the union of multiple rectangular areas.

Region	Latitude		Longitude	
	min	max	min	max
France				
Bordeaux	44.3	46.3	−1.5	0.8
Bourgogne	45.3	47.9	3.3	5.0
Champagne	47.9	49.5	2.5	5.5
Alsace	47.5	48.9	7.0	8.3
Provence	42.9	43.9	4.7	7.4
Loire Valley	46.2	48.5	−2.0	3.3
Corsica	41.5	43.0	8.5	9.7
South-West of France	43.0	44.5	−1.3	1.0
	43.4	45.1	0.9	2.2
Languedoc	42.0	44.2	1.9	4.1
	41.7	44.2	2.8	4.1
Rhone Valley	43.3	45.7	4.0	5.7
Italy				
Tuscany - Roma	42.2	44.3	9.4	12.7
Piedmont	44.3	45.3	7.2	10.0
Aosta Valley	45.3	46.0	7.2	8.1
Sicily	36.5	38.5	12.0	15.5
Apulia	37.7	40.7	14.3	19.0
Trentino-Veneto	44.7	46.2	12.0	13.2
	44.3	46.7	10.2	12.0
Friuli - Venezia - Giulia	44.7	46.3	13.2	14.3
Tuscany - Roma	40.6	42.1	12.0	14.3
Italy - Adriatic	42.0	44.0	12.7	14.5
	40.7	42.2	14.3	19.0
Sardinia	38.5	41.3	8.0	10.0
Iberian Peninsula				
Ribera del Guardiana	38.0	40.0	−7.5	−4.9
Catalonia	40.7	42.5	−0.5	2.5
Castilla - La Mancha	38.4	40.6	−4.9	−2.6
Galicia	41.8	43.0	−9.5	−7.0
Andalusia	36.2	38.4	−6.9	−2.2
Castile and León	40.8	42.8	−6.9	−3.1
Rioja	40.8	42.8	−3.1	0.4
Majorca	39.0	40.0	2.5	3.5
Valencia	37.2	40.2	−2.6	0.4
Southern Portugal	36.8	40.0	−10.0	−7.0
Northern Portugal	40.0	42.2	−8.9	−5.9
Germany and Switzerland				
Wallis	46.0	46.4	6.8	8.0
Western Switzerland	46.0	47.1	5.8	7.2
	45.3	47.5	5.2	6.5
Eastern Switzerland	47.2	47.9	8.0	9.7
Alps	45.3	47.2	8.2	10.4
South-West of Germany	49.4	50.6	5.9	7.5
	48.9	50.4	7.5	10.8
	48.5	49.0	9.0	9.6
Germany - Saale	50.0	52.0	11.4	15.0
Hungary				
Upper Danube Valley	47.5	49.0	16.1	19.5
	48.1	49.3	15.0	17.6
Tisza Valley	47.6	48.9	19.6	22.5
	45.7	48.1	21.0	23.5
Western Hungary	45.8	47.8	16.3	20.5
Mediterranean islands				
Peloponnese	36.0	38.9	20.0	25.7
Crete	34.7	35.7	23.3	26.5
Cyprus	34.0	35.5	32.0	34.6

(*continued on next page*)

Table B.1 (*continued*).

Region	Latitude		Longitude	
	min	max	min	max
Turkey				
Western Turkey	36.4	39.0	25.6	29.0
Northwestern Turkey	39.0	41.5	26.0	33.3
Southern Turkey	36.0	38.8	31.0	36.5
	37.4	38.7	33.4	37.1
Turkey - Isparta	36.4	39.0	29.0	31.0
Southeastern Anatolia	36.0	41.0	36.5	42.0
Northern Anatolia	38.6	42.0	33.4	37.1
Romania				
Transylvania	45.5	47.3	23.1	25.3
Hills of Moldova - North	46.0	48.2	26.0	28.6
Hills of Moldova - South	45.1	46.0	26.0	28.6
Lower Danube Valley	42.9	45.2	22.4	29.5
Balkans				
Balkans	42.8	46.3	18.7	23.1
	42.3	43.5	16.6	18.8
	39.3	42.8	19.0	21.0
Croatian uplands	43.9	46.0	16.7	20.0
Dalmatia	43.0	45.2	14.2	17.3
Thracian Valley - Macedonia	41.3	42.9	23.6	29.5
	38.9	41.6	19.0	25.0
	40.7	42.4	20.30	23.6
Podravska	45.1	47.0	14.3	16.7
Non-wine-growing regions				
Algeria - Tunisia - coast	34.7	37.5	−2.4	11.3
Sahara desert - Algeria	28.0	34.7	−2.4	11.9
Sahara desert - Morocco	27.0	32.4	−10.0	−2.4
Morocco - coast	32.4	35.9	−10.0	−2.4
Sahara desert - Libya	29.7	33.4	9.20	33.0
Middle East	29.5	34.0	32.5	36.9
Georgia	41.0	43.7	40.0	46.5
Syria	33.0	36.0	35.2	42.0
Southern Russia	43.2	46.2	37.0	44.7
Ireland	51.4	55.5	−10.5	−5.3
Southern England	49.9	53.5	−5.9	1.9
Northern England	53.5	56.1	−5.2	0.3
Southern Sweden	55.1	59.6	10.9	17.0
Belarus	51.9	56.5	23.4	32.4
Britanny	47.0	48.9	−4.9	−2.0
Normandie	48.5	50.2	−2.0	2.5
Belgium - Netherlands	49.5	53.4	2.5	5.9
Northwestern Germany	50.5	53.9	5.9	11.4
Northeastern Germany	52.0	54.5	11.4	15.0
Germany - Austria	46.2	50.0	10.0	15.0
	47.2	48.8	8.3	10.0
Southern Poland	48.9	52.5	15.0	23.5
Northern Poland	52.5	56.5	15.0	23.4
Carpathian Mountains	45.2	45.7	23.0	26.0
	45.7	47.3	25.3	26.0
	47.3	48.9	22.5	26.0
Western Ukraine	48.3	51.9	23.5	31.5
Ukraine - Dnieper Valley	45.2	50.2	31.5	36.5
Moldova	45.2	48.3	28.6	31.5
Russia - Volga	46.2	50.3	36.5	44.7
Denmark	53.9	57.8	7.9	10.9
Latvia	55.6	58.2	20.9	28.5

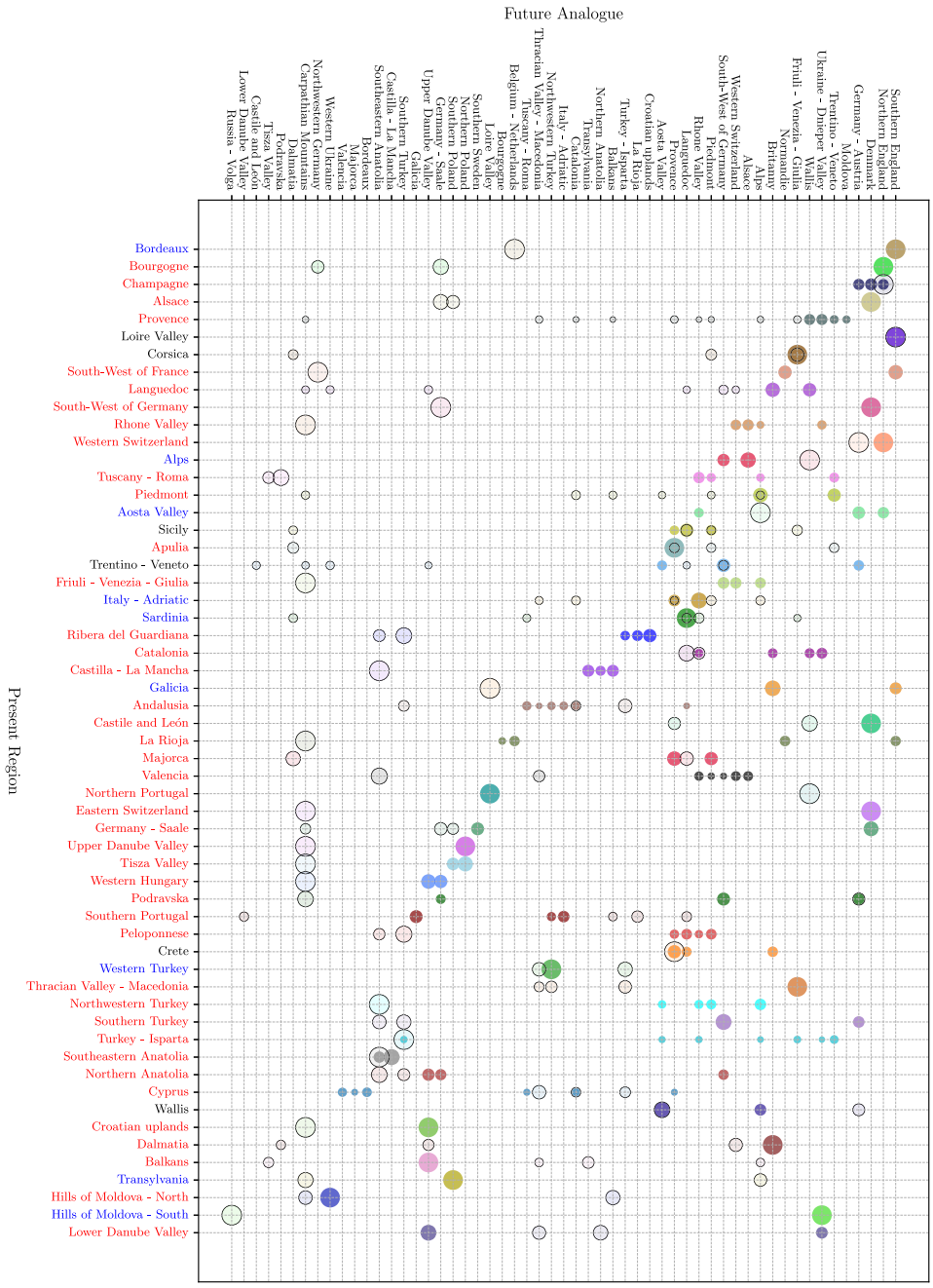

Fig. C.1. Regions matches between wine-growing regions in the present (left) and their prospective analogue regions in the future (top). The area of the dot is proportional to the score of the analogue region. Dark circles: using only temperature-related indices: Huglin index, flavescence dorée, as well as frost and extreme heat days; light circles: using all six bioclimatic indices. Blue present regions: different top analogue ≤ 500 km apart; red present regions: different top analogue > 500 km apart.

References

Abouassaf, Haya, 2013. Studies on Lobesia Botrana and Scaphoideus Titanus for Their Successful Management in Organic and Conventional Viticulture (Ph.D. thesis). Università degli studi di Padova.

Allaman, Héloïse, Goyette, Stéphane, Dubuis, Pierre-Henri, Kasparian, Jérôme, 2025. Climate analogues of European vineyards, Yareta repository with supporting data and code. http://dx.doi.org/10.26037/yareta:5amaf72rdfdd3eb7liq5aya4su.

Bennie, Jonathan, Huntley, Brian, Wiltshire, Andrew, Hill, Mark O., Baxter, Robert, 2008. Slope, aspect and climate: Spatially explicit and implicit models of topographic microclimate in chalk grassland. Ecol. Model. 216 (1), 47–59. http://dx.doi.org/10.1016/j.ecolmodel.2008.04.010, URL https://www.sciencedirect.com/science/article/pii/S0304380008002056.

Bulut, Burak, Vrac, Mathieu, de Noblet-Ducoudré, N., 2025. What will the European climate look like in the future? A climate analog analysis accounting for dependencies between variables. Earth's Futur. 13 (1), http://dx.doi.org/10.1029/2024ef004972, URL https://agupubs.onlinelibrary.wiley.com/doi/10.1029/2024EF004972.

Caffarra, Amelia, Rinaldi, Monica, Eccel, Emanuele, Rossi, Vittorio, Pertot, Ilaria, 2012. Modelling the impact of climate change on the interaction between grapevine and its pests and pathogens: European grapevine moth and powdery mildew. Agric. Ecosyst. Environ. 148, 89–101. http://dx.doi.org/10.1016/j.agee.2011.11.017, URL https://www.sciencedirect.com/science/article/pii/S0167880911003975.

Carroll, J., Wilcox, Wayne, 2003. Effects of humidity on the development of grapevine powdery Mildew. Phytopathology 93, 1137–1144. http://dx.doi.org/10.1094/PHYTO.2003.93.9.1137.

Christensen, Ole, Drews, Martin, Christensen, Jens, Dethloff, Klaus, Hebestadt, Ines, Ketelsen, Klaus, Rinke, Annette, 2007. The HIRHAM regional climate model. Version 5 (beta). DMI Tech. Rep. 06-17.

Chuche, Julien, Thiéry, Denis, 2014. Biology and ecology of the flavescence dorée vector scaphoideus titanus: a review. Agron. Sustain. Dev. http://dx.doi.org/10.1007/s13593-014-0208-7.

Copernicus Land Monitoring Service and European Commission, 2013. European digital elevation model (EU-DEM). URL https://ec.europa.eu/eurostat/web/gisco/geodata/digital-elevation-model/eu-dem, (Accessed: Oct. 2024). Copernicus Land Monitoring Service, European Commission.

De Rességuier, Laure, Mary, Séverine, Le Roux, Renan, Petitjean, Théo, Quénol, Hervé, Van Leeuwen, Cornelis, 2020. Temperature variability at local scale in the Bordeaux area. Relations with environmental factors and impact on vine phenology. Front. Plant Sci. 11, 515. http://dx.doi.org/10.3389/fpls.2020.00515.

Dupin, Séverine, Raynal, Marc, 2024. Le mildiou en 2023: Retours terrain, bilan de l'enquête, travaux menés pour accompagner les viticulteurs et leviers. In: Technical report. Vinopôle Bordeaux Aquitaine, Chambre d'Agriculture de la Gironde.

European Environment Agency, 2018. CORINE land cover 2018 (CLC). http://dx.doi.org/10.2909/960998c1-1870-4e82-8051-6485205ebbac, URL https://land.copernicus.eu/en/products/corine-land-cover/clc2018, (Accessed Oct. 2024).

European Union's Copernicus Land Monitoring Service, 2025. Copernicus land cover data viewer. URL https://land.copernicus.eu/en/map-viewer?dataset=0407d497d3c44bcd93ce8fd5bf78596a, (Accessed: March 2025).

Fennell, Anne, 2004. Freezing tolerance and injury in grapevines. J. Crop. Improv. 10, 201–235. http://dx.doi.org/10.1300/J411v10n01_09.

Fessler, C., Kassemeyer, H.H., 1995. The influence of temperature during the development of conidia on the germination of Uncinula necator. Vitis 34 (1), 63–64.

Francesca, Salinari, Giosuè, Simona, Tubiello, Francesco, Andrea, Rettori, Rossi, Vittorio, Federico, Spanna, Cynthia, Rosenzweig, Gullino, Maria, 2006. Downy mildew (Plasmopara viticola) epidemics on grapevine under climate change. Global Change Biol. 12, 1299–1307. http://dx.doi.org/10.1111/j.1365-2486.2006.01175.x.

Gaponenko, Iaroslav, Rohat, Guillaume, Goyette, Stéphane, Paruch, Patrycja, Kasparian, Jérôme, 2022. Smooth velocity fields for tracking climate change. Sci. Rep. 12 (1), 2997. http://dx.doi.org/10.1038/s41598-022-07056-z.

Garcia de Cortazar-Atauri, Iñaki, Brisson, Nadine, Gaudillere, Jean, 2009. Performance of several models for predicting budburst date of grapevine (Vitis vinifera L.). Int. J. Biometeorol. 53, 317–326. http://dx.doi.org/10.1007/s00484-009-0217-4.

Hall, Andrew, Jones, Gregory V., 2010. Spatial analysis of climate in winegrape-growing regions in Australia. Aust. J. Grape Wine Res. 16 (3), 389–404. http://dx.doi.org/10.1111/j.1755-0238.2010.00100.x.

Huglin, Pierre, 1986. Biologie et écologie de la vigne. Paris, Lavoisier - Tec & doc.

Jacob, Daniela, Bärring, Lars, Christensen, Ole Bøssing, Christensen, Jens Hesselbjerg, de Castro, Manuel, Déqué, Michel, Giorgi, Filippo, Hagemann, Stefan, Hirschi, Martin, Jones, Richard, et al., 2007. An inter-comparison of regional climate models for Europe: model performance in present-day climate. Clim. Change 81, 31–52.

Jacob, Daniela, Petersen, Juliane, Eggert, Bastian, Alias, Antoinette, Christensen, Ole, Bouwer, Laurens, Braun, Alain, Colette, Augustin, Déqué, Michel, Georgievski, Goran, Georgopoulou, Elena, Gobiet, Andreas, Menut, Laurent, Nikulin, Grigory, Haensler, Andreas, Hempelmann, Nils, Jones, Colin, Keuler, Klaus, Kovats, Sari, Yiou, Pascal, 2014. EURO-CORDEX: New high-resolution climate change projections for European impact research. Reg. Environ. Chang. 14, http://dx.doi.org/10.1007/s10113-013-0499-2, URL https://esgf-ui.ceda.ac.uk/cog/search/cordex-ceda/.

Jones, Gregory V., Reid, Ryan, Vilks, Aleksander, 2012. Climate, grapes, and wine: Structure and suitability in a variable and changing climate. In: The Geography of Wine: Regions, Terroir and Techniques. Springer Netherlands, Dordrecht, pp. 109–133. http://dx.doi.org/10.1007/978-94-007-0464-0_7, URL http://dx.doi.org/10.1007/978-94-007-0464-0_7.

Keller, Markus, 2020. The Science of Grapevines, Third Edition. Elsevier Inc..

van Leeuwen, Cornelis, Darriet, Philippe, 2016. The impact of climate change on viticulture and wine quality. J. Wine Econ. 11 (1), 150–167. http://dx.doi.org/10.1017/jwe.2015.21.

Loarie, Scott R, Duffy, Philip B, Hamilton, Healy, Asner, Gregory P, Field, Christopher B, Ackerly, David D, 2009. The velocity of climate change. Nature 462 (7276), 1052–1055. http://dx.doi.org/10.1038/nature08649.

Magdić, Ivan, Safner, Toni, Rubinić, Vedran, Rutić, Filip, Husnjak, Stjepan, Filipović, Vilim, 2022. Effect of slope position on soil properties and soil moisture regime of stagnosol in the vineyard. J. Hydrol. Hydromechanics 70 (1), 62–73. http://dx.doi.org/10.2478/johh-2021-0037.

Malheiro, Aureliano C, Santos, João A, Fraga, Helder, Pinto, Joaquim G, 2010. Climate change scenarios applied to viticultural zoning in Europe. Clim. Res. 43 (3), 163–177. http://dx.doi.org/10.3354/cr00918.

Mozell, Michelle Renée, Thach, Liz, 2014. The impact of climate change on the global wine industry: Challenges & solutions. Wine Econ. Policy 3 (2), 81–89. http://dx.doi.org/10.1016/j.wep.2014.08.001, URL https://www.sciencedirect.com/science/article/pii/S2212977414000222.

Nesbitt, A., Dorling, S., Lovett, A., 2018. A suitability model for viticulture in England and Wales: opportunities for investment, sector growth and increased climate resilience. J. Land Use Sci. 13 (4), 414–438. http://dx.doi.org/10.1080/1747423X.2018.1537312.

Oke, Timothy R., 1987. Boundary Layer Climates. Routledge.

Olivier Viret, Katia Gindro, 2025. Science of Fungi in Grapevine. Springer Nature, http://dx.doi.org/10.1007/978-3-031-68663-4.

Peixoto, J.P., Oort, A.H., 1992. Physics of Climate. New York, NY (United States); American Institute of Physics, URL https://www.osti.gov/biblio/7287064.

Pieri, P., Gaudillère, J.P., 2015. Sensitivity to training system parameters and soil surface albedo of solar radiation intercepted by vine rows. VITIS - J. Grapevine Res. 42 (2), 77. http://dx.doi.org/10.5073/vitis.2003.42.77-82, URL https://ojs.openagrar.de/index.php/VITIS/article/view/4395.

Piña-Rey, Alba, González-Fernández, Estefanía, Fernández-González, María, Lorenzo, M^{a}. Nieves, Rodríguez-Rajo, Fco. Javier, 2020. Climate change impacts assessment on wine-growing bioclimatic transition areas. Agriculture 10 (12), http://dx.doi.org/10.3390/agriculture10120605, URL https://www.mdpi.com/2077-0472/10/12/605.

Poling, E. Barclay, 2008. Spring cold injury to winegrapes and protection strategies and methods. HortScience 43 (6), 1652–1662. http://dx.doi.org/10.21273/HORTSCI.43.6.1652, URL https://journals.ashs.org/hortsci/view/journals/hortsci/43/6/article-p1652.xml.

QGIS, 2024. QGIS geographic information system. URL www.qgis.org, Open Source Geospatial Foundation Project, https://qgis.org.

Ramírez Villegas, Julián Armando, Lau, Charlotte, Köhler, Ann-Kristin, Jarvis, Andy, Arnell, NP, Osborne, Tom M, Hooker, Josh, 2011. Climate Analogues: Finding Tomorrow's Agriculture Today. CGIAR Research Program on Climate Change, Agriculture and Food Security.

Rigamonti, Ivo E, Jermini, Mauro, Fuog, Daniele, Baumgärtner, Johann, 2011. Towards an improved understanding of the dynamics of vineyard-infesting scaphoideus titanus leafhopper populations for better timing of management activities. Pest. Manag. Sci. 67, 1222–1229. http://dx.doi.org/10.1002/ps.2171.

Robert, Steffek, Reisenzein, Helga, Strauss, Gudrun, Leichtfried, Thomas, Hofrichter, Johannes, Kopacka, Ian, Schwarz, Michael, Pusterhofer, Josef, Biedermann, Reinhold, Renner, Wolfgang, Klement, Josef, Luttenberger, Werner, Welzl, Alexander, Kleissner, Anna, Alt, Raimund, 2011. VitisCLIM, a project modelling epidemiology and economic impact of grapevine 'flavescence dorée' phytoplasma in Austrian viticulture under a climate change scenario. Bull. Insectology 64, 191–192.

Rohat, Guillaume, Goyette, Stéphane, Flacke, Johannes, 2017. Characterization of European cities' climate shift – an exploratory study based on climate analogues. Int. J. Clim. Chang. Strat. Manag. 10 (3), 428–452. http://dx.doi.org/10.1108/IJCCSM-05-2017-0108, URL https://www.sciencedirect.com/science/article/pii/S1756869218000169.

Sneiders, B., Fleury, D., Goyette, S., 2019. Influence du réchauffement climatique sur la dynamique des populations de scaphoideus titanus en romandie. Rev. Suisse Vitic. Arboric. Hortic..

Stillson, Patrick T, Bloom, Elias H, Illán, Javier G, Szendrei, Zsofia, 2020. A novel plant pathogen management tool for vector management. Pest. Manag. Sci. 76 (11), 3729–3737. http://dx.doi.org/10.1002/ps.5922.

Strub, Larissa, Loose, Simone Mueller, 2021. The cost disadvantage of steep slope viticulture and strategies for its preservation. Oeno One 55 (1), 49–68.

Ungar, Joachim, Peters-Anders, Jan, Loibl, Wolfgang, 2011. Climate twins – An attempt to quantify climatological similarities. IFIP Adv. Inf. Commun. Technol. 359, 428–436. http://dx.doi.org/10.1007/978-3-642-22285-6_46.

Venios, Xenophon, Korkas, Elias, Nisiotou, Aspasia, Banilas, Georgios, 2020. Grapevine responses to heat stress and global warming. Plants 9 (12), http://dx.doi.org/10.3390/plants9121754, URL https://www.mdpi.com/2223-7747/9/12/1754.

Vidal, René, Ma, Yanlai, Sastry, Shankar, 2012. Generalized principal component analysis. 27, Springer,

Walter Kast, K. Bleyer, 2009. The expert system OiDiag-2.2. - a useful tool for the precise scheduling of sprays against powdery mildew of vine (Erysiphe necator Schwein). State Inst. Vitic. Oenology Fruit Technol..

Wann, Mien, Yen, Doreen, Gold, Harvey J., 1985. Evaluation and calibration of three models for daily cycle of air temperature. Agricult. Forest. Meterol. 34 (2), 121–128. http://dx.doi.org/10.1016/0168-1923(85)90013-9, URL https://www.sciencedirect.com/science/article/pii/0168192385900139.

Webb, Leanne, Watterson, I., Bhend, Jonas, Whetton, Penny, Barlow, Edward, 2013. Global climate analogues for winegrowing regions in future periods: Projections of temperature and precipitation. Aust. J. Grape Wine Res. 19, http://dx.doi.org/10.1111/ajgw.12045.

Zito, S., Castel, T., Richard, Y., Rega, M., Bois, B., 2020. Optimization of a leaf wetness duration model. Agricult. Forest. Meterol. 291, 108087. http://dx.doi.org/10.1016/j.agrformet.2020.108087, URL https://www.sciencedirect.com/science/article/pii/S0168192320301891.

Zito, Sébastien, Richard, Yves, Castel, Thierry, Bois, Benjamin, 2019. Impact du changement climatique sur l'oïdium de la vigne : cas de la champagne. Bourgogne-Franche-ComtÉ Nat. 206–212.